JEM Journal of Experimental Medicine

ARTICLE

Primary tumor–derived systemic nANGPTL4 inhibits metastasis

Corinne Hübers[1,2,3*], Ashik Ahmed Abdul Pari[1,2,4*], Denise Grieshober[1,2,4*], Martin Petkov[1,2], Alexander Schmidt[5], Tatjana Messmer[2,3], Christian Moritz Heyer[4,6], Sebastian Schölch[7,8,9], Stephanie S. Kapel[1,2], Nicolas Gengenbacher[1,2], Mahak Singhal[1,2,10], Benjamin Schieb[1,2], Claudine Fricke[1,2], Rainer Will[11], Kim Remans[12], Jochen Sven Utikal[3,13], Christoph Reissfelder[8,9], Matthias Schlesner[6], Kairbaan M. Hodivala-Dilke[14], Sander Kersten[15], Sergij Goerdt[1,3], Hellmut G. Augustin[1,2**], and Moritz Felcht[1,2,3**]

Primary tumors and distant site metastases form a bidirectionally communicating system. Yet, the molecular mechanisms of this crosstalk are poorly understood. Here, we identified the proteolytically cleaved fragments of angiopoietin-like 4 (ANGPTL4) as contextually active protumorigenic and antitumorigenic contributors in this communication ecosystem. Preclinical studies in multiple tumor models revealed that the C-terminal fragment (cANGPTL4) promoted tumor growth and metastasis. In contrast, the N-terminal fragment of ANGPTL4 (nANGPTL4) inhibited metastasis and enhanced overall survival in a postsurgical metastasis model by inhibiting WNT signaling and reducing vascularity at the metastatic site. Tracing ANGPTL4 and its fragments in tumor patients detected full-length ANGPTL4 primarily in tumor tissues, whereas nANGPTL4 predominated in systemic circulation and correlated inversely with disease progression. The study highlights the spatial context of the proteolytic cleavage-dependent pro- and antitumorigenic functions of ANGPTL4 and identifies and validates nANGPTL4 as a novel biomarker of tumor progression and antimetastatic therapeutic agent.

Introduction

Cancer has become the leading cause of death in high-income countries (Dagenais et al., 2020). While primary tumors can mostly be controlled in industrialized countries with advanced healthcare systems, most patients succumb to distant site metastases (Dillekas et al., 2019). Existing therapeutic regimes are mainly designed to curb primary tumor growth and have limited efficacy in patients with metastases (Stoletov et al., 2020). A better molecular and mechanistic understanding of metastasis is therefore urgently needed to identify unappreciated vulnerabilities in the metastasis program and to develop novel therapeutic regimens.

The classic concept of metastasis formation is that of a metastatic cascade, whereby dissemination of tumor cells may occur early and at high frequency, whereas colonization and the formation of macroscopic metastases occur relatively late and at a much lower frequency (Welch and Hurst, 2019). Clinically, these late steps of the metastatic cascade are most crucial for the patient's outcome. Another concept focuses on the delay in macroscopic metastases formation and has been termed "concomitant tumor resistance" (CTR), the active inhibition of metastatic growth through signals derived from the primary tumor. Several preclinical and clinical studies have highlighted the importance of CTR in controlling metastatic outgrowth (Chiarella et al., 2012). For example, in breast and melanoma cancer models, mice bearing primary tumors had reduced metastatic dissemination in the lungs compared with non-

[1]European Center for Angioscience, Medical Faculty Mannheim, Heidelberg University, Mannheim, Germany; [2]Division of Vascular Oncology and Metastasis, German Cancer Research Center (DKFZ-ZMBH Alliance), Heidelberg, Germany; [3]Department of Dermatology, Venereology and Allergy, University Medical Centre Mannheim, Medical Faculty Mannheim, Heidelberg University and Centre of Excellence of Dermatology of Baden-Württemberg, Mannheim, Germany; [4]Faculty of Biosciences, Heidelberg University, Heidelberg, Germany; [5]Department of Biomedicine, University of Basel, Basel, Switzerland; [6]Biomedical Informatics, Data Mining and Data Analytics, Augsburg University, Augsburg, Germany; [7]JCCU Translational Surgical Oncology (A430), German Cancer Research Center, Heidelberg, Germany; [8]Department of Surgery, University Medical Centre Mannheim, Medical Faculty Mannheim, Heidelberg University, Mannheim, Germany; [9]DKFZ-Hector Cancer Institute at University Medical Centre Mannheim, Mannheim, Germany; [10]Laboratory of AngioRhythms, European Center for Angioscience, Medical Faculty Mannheim, Heidelberg University, Mannheim, Germany; [11]Genomics & Proteomics Core Facilities, German Cancer Research Center, Heidelberg, Germany; [12]Protein Expression and Purification Core Facility, European Molecular Biology Center, Heidelberg, Germany; [13]Skin Cancer Unit, German Cancer Research Center, Heidelberg, Germany; [14]Center for Tumor Biology, Barts Cancer Institute, Queen Mary University of London, John Vane Science Center, London, United Kingdom; [15]Nutrition, Metabolism and Genomics group, Division of Human Nutrition and Health, Wageningen University, Wageningen, The Netherlands.

*C. Hübers, A.A. Abdul Pari, and D. Grieshober contributed equally to this paper; **H.G. Augustin and M. Felcht contributed equally to this paper. Correspondence to Hellmut G. Augustin: augustin@angioscience.de; Moritz Felcht: moritz_felcht@gmx.de.

tumor-bearing mice (Kubo et al., 2017; O'Reilly et al., 1994; Piranlioglu et al., 2019). These preclinical findings are supported by clinical observations demonstrating that breast cancer and melanoma metastases occur in the majority of patients only after resection of the primary tumor (Alieva et al., 2018; Meier et al., 2002; Tohme et al., 2017). Yet, the underlying mechanisms of CTR continue to be poorly understood. Emerging evidence suggests that CTR is controlled by at least two mechanisms (Chiarella et al., 2012), the host's immune system and systemically acting primary tumor–released antimitogenic and/or antiangiogenic cytokines (Folkman, 2006; Krall et al., 2018; Tohme et al., 2017).

The concepts of CTR were experimentally pioneered more than two decades ago when primary tumors were first identified to produce both proangiogenic and antiangiogenic cytokines that regulate primary tumor growth and metastatic colonization in a context-dependent manner (O'Reilly et al., 1997; O'Reilly et al., 1994). According to these early discoveries, proangiogenic molecules were believed to be short-lived and locally acting, whereas antiangiogenic molecules were proposed to be long-lived and systemically acting. Thereby, the proangiogenic milieu may predominate locally in the primary tumor to support its growth, whereas primary tumor–derived antiangiogenic activity may affect systemic homeostasis to effectively limit distant site metastatic colonization. The proposed contextuality of local proangiogenic and systemic antiangiogenic activities provided a compelling model for opposing growth-stimulating and growth-inhibiting activities originating from the primary tumor. It also provided a plausible mechanistic explanation for the observed growth of metastases following surgical removal of the primary tumor (Folkman, 2006; Hanahan and Folkman, 1996). Moreover, the activity of several endogenous inhibitors of angiogenesis, including thrombospondin and endostatin, was also validated in definite genetic experiments (Sund et al., 2005). Yet, efforts to exploit endogenous inhibitors of angiogenesis as therapeutic agents have failed so far (Rao et al., 2015).

Angiopoietin-like protein 4 (ANGPTL4) is a secreted glycoprotein belonging to a family of nine structurally similar ANGPTL proteins (Costa et al., 2017). ANGPTL4 has been characterized as the stimulator of angiogenesis, thereby acting as a crucial regulator of cancer progression (Chiang and Massagué, 2008; La Paglia et al., 2017). However, the published literature on ANGPTL4 functions during tumor progression is highly controversial. While the majority of studies portray ANGPTL4 as a proangiogenic and protumorigenic molecule (Baba et al., 2017; Chen et al., 2018; Hu et al., 2016; Huang et al., 2011; Izraely et al., 2017; Kolb et al., 2019; Le Jan et al., 2003; Li et al., 2011; Li et al., 2015; Liao et al., 2017; Ma et al., 2010; Padua et al., 2008; Tian et al., 2009; Zhang et al., 2018; Zhu et al., 2011), there is a considerable body of evidence ascribing antiangiogenic (Cazes et al., 2006; Galaup et al., 2012; Gomez Perdiguero et al., 2016) and antitumorigenic activities on ANGPTL4 (Galaup et al., 2006; Ng et al., 2014; Okochi-Takada et al., 2014). These conflicting reports led us to reconsider ANGPTL4 in light of the concepts of CTR to hypothesize that ANGPTL4 may contextually exert both protumorigenic and antitumorigenic functions. Specifically, ANGPTL4 has been shown to be proteolytically cleaved upon secretion into two fragments, an N-terminal (nANGPTL4) and a C-terminal (cANGPTL4) fragment. Both fragments are functional, with the N-terminal fragment being shown to inhibit lipoprotein lipase (LPL) activity and to reduce circulating triglycerides levels, whereas the C-terminal fragment is integrin-binding and acts as a stimulator of angiogenesis (Tan et al., 2012). In addition, cANGPTL4 has been described as a vasoactive agent in the context of ocular neovascular disease (Qin et al., 2022; Sodhi et al., 2019; Yang et al., 2018). We consequently hypothesized that proteolytic processing may act as a regulator of ANGPTL4 pro- and antitumorigenic functions. Indeed, tracing ANGPTL4 in human tumor patients detected local full-length uncleaved ANGPTL4 in tumor specimens, whereas cleaved nANGPTL4 predominated in the systemic circulation of cancer patients. Using a battery of in vitro, ex vivo, and in vivo assays, we established that full-length ANGPTL4 and cANGPTL4 act as proangiogenic and protumorigenic cytokines. In contrast, systemic nANGPTL4 inhibited sprouting angiogenesis and suppressed distant site metastasis. The translational relevance of these findings was validated by demonstrating that recombinant nANGPTL4 potently reduced macrometastatic growth in preclinical models and by showing that serum nANGPTL4 levels in melanoma patients correlated inversely with disease progression.

Results

Expression of ANGPTL4 and its fragments differs between primary tumor tissue and the circulation

The balance of pro- and antiangiogenic factors produced by the primary tumor has been shown to critically control CTR (Chiarella et al., 2012). We, therefore correlated the expression profile of 38 highly expressed angiogenic factors with patient survival in 32 tumor entities. This screen identified ANGPTL4 among the angiogenic molecules most significantly correlating inversely with patient survival (Fig. 1 A and Fig. S1, A–F). To substantiate these findings, ANGPTL4 protein levels were immunohistochemically compared in tissue microarrays (TMAs) of six common tumor entities (n = 30–180) with their healthy counterparts (each n = 7–30; Fig. 1 B and Fig. S2, A–C). ANGPTL4 was more abundantly detectable in primary tumor biopsies when compared with corresponding healthy tissues. Importantly, ANGPTL4 expression in primary tumor biopsies was mainly observed in tumor cells. Comparative analysis of ANGPTL4 expression among different grades of colon carcinoma, squamous cell carcinoma (SCC), and melanoma patient samples demonstrated that ANGPTL4 expression correlated positively with tumor progression (Fig. 1 C). These data identify tumor cells as the primary source of ANGPTL4 in the tumor microenvironment and suggest a role of ANGPTL4 as a negative prognostic factor for tumor progression, corresponding to reports that serum levels of ANGPTL4 correlate with cancer prognosis (La Paglia et al., 2017; Tan et al., 2012).

ANGPTL4 protein is proteolytically cleaved at its ^{161}RKRR^{164} site into a C- and N-terminal fragment (cANGPTL4, nANGPTL4; Fig. S2 D). Several studies have suggested distinct functions of the ANGPTL4 cleavage fragments (La Paglia et al., 2017; Tan

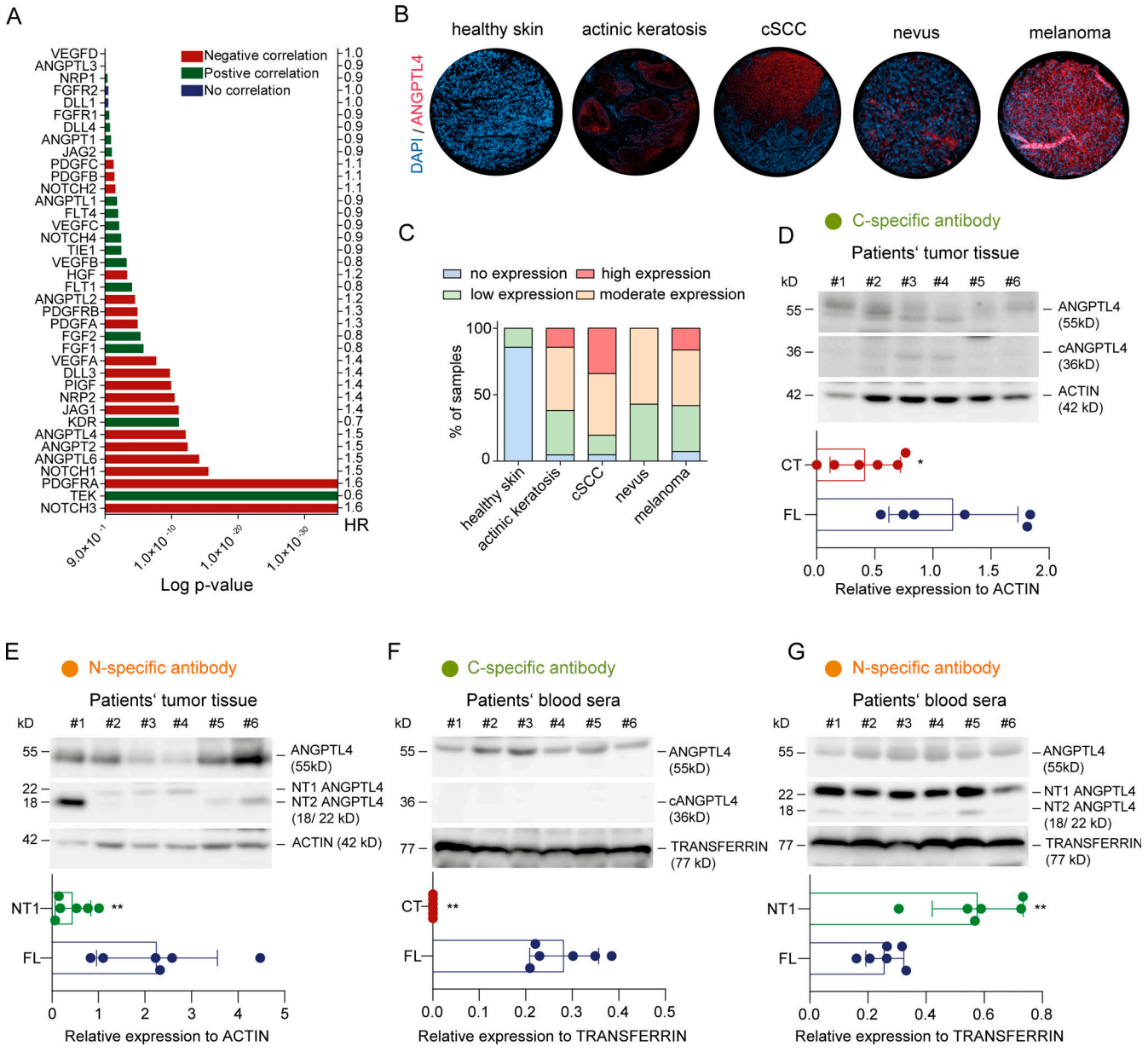

Figure 1. **Tracing the distribution of ANGPTL4 and its fragments in local tumor tissues and serum samples from melanoma patients. (A)** Graph depicts the significance (log-rank [Mantel–Cox] test) of Kaplan–Meier plots comparing high (>75 percentile) and low (<25 percentile) gene expression of 38 angiogenic molecules with overall survival of patients from 32 cancer entities. HR, hazard ratio. **(B)** Representative immunofluorescent (IF) images of heathy skin, AK, primary cutaneous SCCs (cSCC), nevus, and melanoma tissue sections stained with ANGPTL4 antibody. **(C)** Quantitation of no, low, moderate, and high ANGPTL4 protein expression in healthy skin (n = 7), AK (n = 107), cSCC (n = 130), nevus (n = 7), and melanoma (n = 160) tissue sections. **(D–G)** Top: Western blotting with a cANGPTL-4–specific antibody (D and F) and a nANGPTL-4–specific antibody (E and G) in indexed melanoma tumors (D and E) and serum samples (F and G). Bottom: Graphs showing the densitometry quantitation of protein levels of the corresponding Western blots. Protein levels were normalized to actin in melanoma tumors and to transferrin in patients' sera (n = 6; mean ± SD). *, P < 0.05; **, P < 0.01, Mann–Whitney U test. Source data are available for this figure: SourceData F1.

et al., 2012). Thus, the distribution of ANGPTL4 and its cleavage fragments may be an important modulator of ANGPTL4 function during tumor progression. To this end, indexed melanoma tumor tissue and blood samples were analyzed with antibodies against specific epitopes in the C and N domains (Fig. S2 D). Abundant ANGPTL4 as well as varying amounts of cANGPTL4 and nANGPTL4 were detected in all tumor tissue samples (Fig. 1, D and E). Similarly, ANGPTL4 was detected in all analyzed serum samples using the C-specific antibody (Fig. 1 F). Yet, patient sera lacked the detectable cANGPTL4 fragment (>50 ng/ml; Fig. 1 F). Western blot analysis with the N-specific antibody detected in all analyzed serum samples ANGPTL4 as well as two distinct forms of nANGPTL4 with an approximate size difference of about 3–4 kD, corresponding to previous studies reporting two different forms (NT1 and NT2) of nANGPTL4, originating from posttranslational modification (Mandard et al.,

2004). Intriguingly, quantitative analysis of melanoma patient serum samples identified significantly higher levels of nANGPTL4 than ANGPTL4 (Fig. 1 G and Fig. S2 E). Likewise, nANGPTL4 was profoundly present in the systemic circulation compared with primary tumor tissue, whereas cANGPTL4 was mainly found in primary tumor tissues and absent in the circulation of lung cancer patients (Fig. S2, F and G). To confirm the presence of ANGPTL4 and nANGPTL4 as well as the absence of cANGPTL4 in the circulation of an independent cohort of cancer patients, we additionally probed a set of 13 melanoma patient serum samples with C- and N-terminal–specific ANGPTL4 antibodies. Indeed, patient serum samples exclusively contained ANGPTL4 and nANGPTL4 (Fig. S2, H and I). Taken together, the data establish the predominant presence of uncleaved ANGPTL4 within primary tumors, whereas the systemic circulation preferentially contained nANGPTL4.

Serum nANGPTL4 levels correlate inversely with disease progression

To determine whether nANGPTL4 serum levels are associated with disease progression, we performed a limited-size prospective longitudinal study on circulating nANGPTL4 levels in melanoma patients. Serum samples were collected from 10 melanoma patients during postoperative clinical visits. Disease progression was regularly monitored by radiological examination and quantitation of serum S100 levels (Fig. 2, A and B; and Fig. S2 J). All patients had suffered from metastatic disease after initial surgical excision of the primary tumor. Interestingly, these metastatic lesions did not progress and remained stable for a longer period of time, defined as stable disease. Yet eventually, metastatic burden increased, and the patients succumbed to metastatic growth. Western blot analyses of stable and progressive disease melanoma patients' serum samples with an nANGTPL4-specific antibody revealed that serum ANGPTL4 levels did not differ between the disease stages (Fig. 2 C, Fig. S2 K, and Table S1). In contrast, serum nANGPTL4 levels significantly dropped with disease progression (Fig. 2, C–E). In line, longitudinal analysis of the NT/ANGPTL4 ratio in a larger cohort of metastatic melanoma patients showed that a decline in NT/ANGPTL4 ratio during disease progression correlated with worse overall survival (Fig. 2, F and G; and Table S1). Overall, the data suggest that serum nANGPTL4 in melanoma patients could contribute to delaying metastatic tumor progression.

Tumor cell–derived ANGPTL4 enhances tumorigenesis

To examine the functional role of ANGPTL4 in the tumor microenvironment, we screened a panel of 4 murine and 19 human tumor cell lines to determine their endogenous *ANGPTL4* expression levels (Fig. S2, L and M). The majority of the screened tumor cell lines (19/23) expressed detectable levels of *ANGPTL4* mRNA. Given the relatively high endogenous expression of *ANGPTL4* in A375 melanoma cells, further detailed analyses were performed with this cell line. *ANGPTL4* expression was stably downregulated in these cells using two independent shRNAs (Fig. S2 N). Next, we subcutaneously implanted parental and *ANGPTL4*-silenced A375 cells in NOD/SCID mice. Silencing of *ANGPTL4* in A375 cells significantly impaired tumor growth (Fig. 3 A). Tumor cell proliferation was not significantly different in control and *ANGPTL4*-silenced tumor cells (Fig. S2 O), which prompted us to examine the vascular architecture in control and *ANGPTL4*-silenced tumors (Fig. 3 B and Fig. S2 P). Immunofluorescence analysis of endothelial cell (EC) marker CD31 in primary tumor tissue sections unveiled a significant decrease in the vascularized area in *ANGPTL4*-silenced tumors compared with control tumors (Fig. 3 C). Correspondingly, recombinant ANGPTL4 enhanced vascular endothelial growth factor A (VEGF-A)–induced sprouting angiogenesis in an in vitro spheroid-based angiogenesis assay (Fig. S3, A–D) as well as in the ex vivo aortic ring assay (Fig. S3, E and F), confirming the in vivo ANGPTL4 loss-of-function data. Together, the data validated the angiogenesis-inducing and tumor-promoting functions of ANGPTL4.

ANGPTL4 enhances tumor angiogenesis via its C domain

Next, we examined if the proangiogenic and protumorigenic functions of ANGPTL4 were modulated by proteolytic processing of ANGPTL4. Toward this end, we performed gain-of-function experiments in two syngeneic mouse tumor models. cANGPTL4 and nANGPTL4 were ectopically expressed in mouse Lewis lung carcinoma (LLC) and melanoma (B16F10) cell lines, which had low levels of endogenous *ANGPTL4* (Fig. S3, G and H). While expression of cANGPTL4 in LLC led to increased primary tumor growth, nANGPTL4 expression had no effect on tumor growth compared with control tumors (Fig. 3 D). Expression of cANGPTL4 and nANGPTL4 in LLC did not affect cellular proliferation, excluding a role on tumor cell proliferation in promoting tumor growth (Fig. S3 I). Instead, expression of cANGPTL4 resulted in an enhanced vascularized area in LLC tumors compared with control tumors. In contrast, expression of nANGPTL4 in LLC had no effect on the intertumoral vasculature (Fig. 3, E and F). To assess the maturation status of the tumor vasculature, we costained tissue sections from control, cANGPTL4-, and nANGPTL4-expressing LLC tumors with CD31 and the mural cell marker Desmin. Quantitation of the percentage of Desmin-positive vessels revealed no significant difference between control, cANGPTL4-, and nANGPTL4-expressing LLC primary tumors (Fig. S3 J).

In the B16F10 melanoma model, cANGPTL4 expression promoted tumor growth in the early stages of tumor development but did not affect later stages of tumor progression (Fig. S3 K). In line with the results obtained in the LLC tumor model, nANGPTL4 expression in B16F10 cells had no significant effect on tumor growth compared with control tumors (Fig. S3 K). Evaluation of cellular proliferation showed no difference between control and ANGPTL4 cleavage fragments expressing B16F10 cells (Fig. S3 L). Instead, examination of the tumor vasculature revealed an increased vascularized area in cANGPTL4-expressing tumors (Fig. S3, M and N). Further, evaluation of perivascular coverage identified a significant reduction of Desmin-positive vessels in cANGPTL4-grafted primary tumors. In contrast, nANGPTL4 expression in B16F10 tumor cells did not affect the vascularized area and perivascular coverage of the tumor vasculature (Fig. S3, M–O). Collectively, these experiments revealed that the proangiogenic and protumorigenic effects of ANGPTL4 were mediated by the C-terminal domain of ANGPTL4.

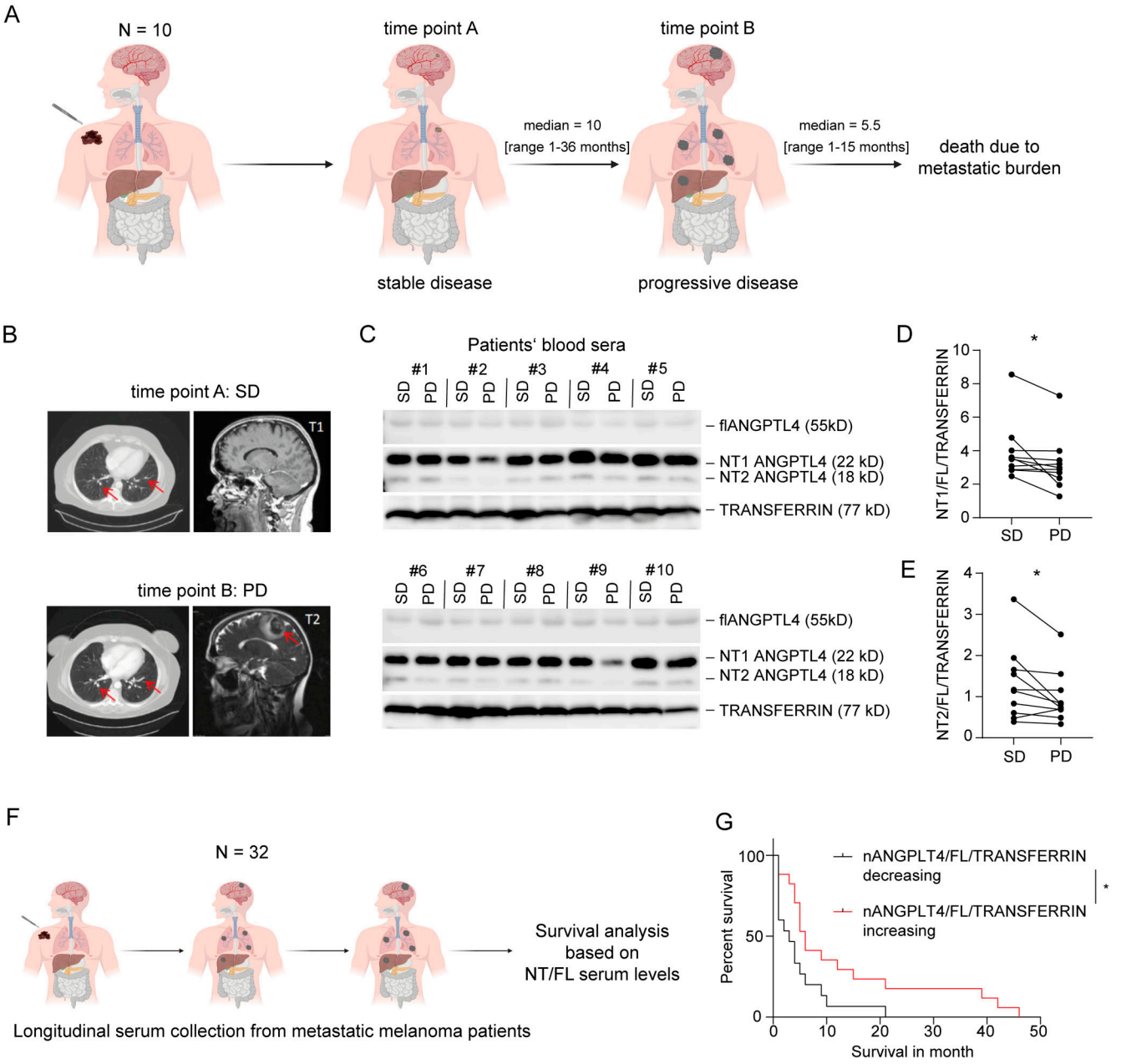

Figure 2. **nANGPTL4 levels decrease in melanoma patients in the transition from stable to progressive disease. (A)** Schematic representation of patient status at time point A (stable disease) and B (progressive disease). The primary melanoma is colored in black. Micrometastases are multicolored, and macrometastases are colored in black. The figure was generated with BioRender.com. **(B)** Representative MRI images of melanoma patients with either stable or progressive disease status. Arrows are pointing toward metastatic areas which are progressing from stable disease (SD) to progressive disease (PD). **(C)** Western blotting with an nANGPTL4-specific antibody in serum samples of melanoma patients with either stable or progressive disease status. Densitometry quantitation of protein levels on Western blot was performed with Fiji. **(D and E)** The graphs show the level of ANGPTL4 (D) and NT1/ANGPTL4 ratio (E) normalized to transferrin in patients' sera with either stable disease or progressive disease diagnosis (n = 10). *, $P < 0.05$, two-tailed paired Student's t test. **(F)** Schematic representation of patient status during longitudinal serum collection. The primary melanoma and macrometastases are colored in black. The figure was generated with BioRender.com. **(G)** Kaplan–Meier plot showing the survival of patients with an increasing or decreasing nANGPTL4/FL ratio. Survival is given as months after the second serum sample was taken (time point B). n = 15–17; *, $P < 0.05$, log-rank (Mantel–Cox) test. Source data are available for this figure: SourceData F2.

Opposing effects of cANGPTL4 and nANGPTL4 during sprouting angiogenesis

The distinct functions of cANGPTL4 and nANGPTL4 on primary tumor growth and vascularization led us to hypothesize that the observed phenotypes might have resulted from different effects of nANGPTL4 and cANGPTL4 on the angiogenic program. We therefore performed spheroid sprouting assays with human umbilical vein ECs (HUVECs) in the presence of the master regulator of the angiogenic cascade VEGF-A (Fig. 4 A and Fig. S3, P and Q). Mono-stimulation with ANGTPL4 or cANGPTL4 induced weak, but consistently detectable vascular sprouting. However, the combination of low-dose VEGF-A and ANGPTL4 or

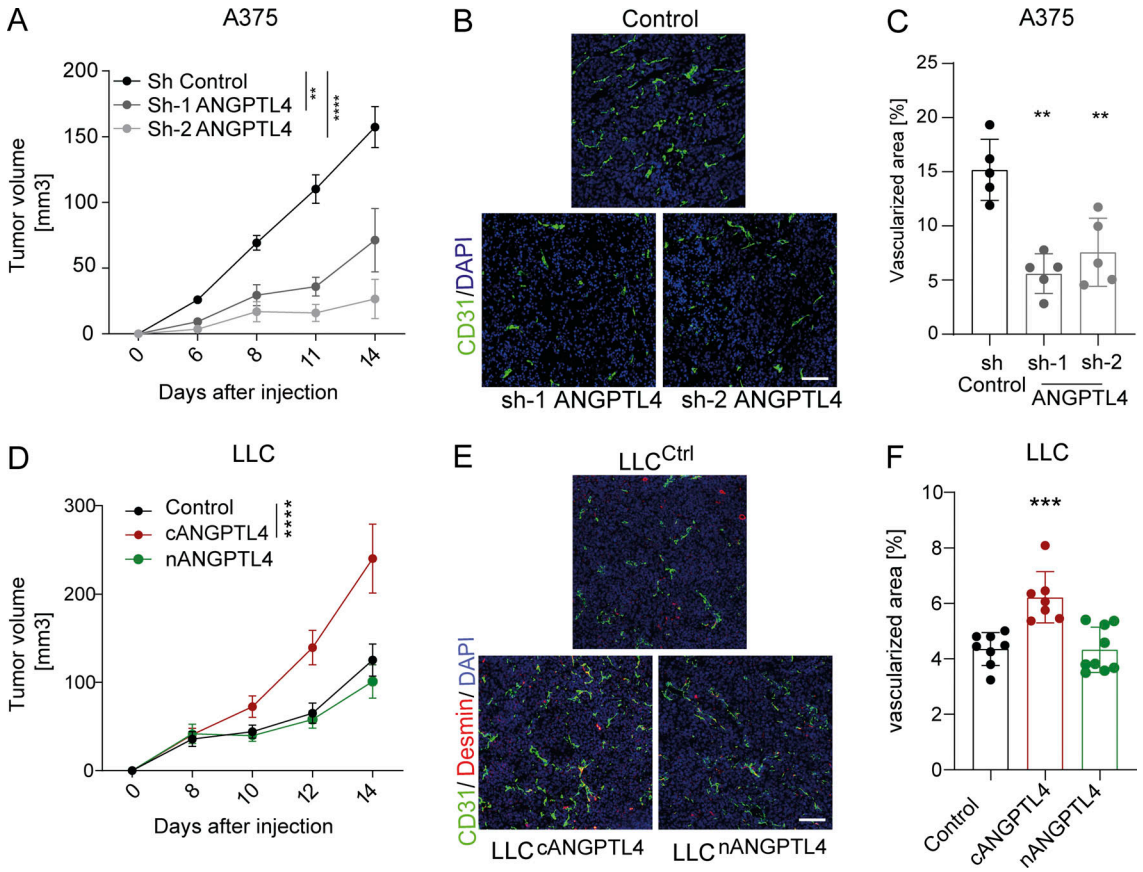

Figure 3. **ANGPTL4 enhances angiogenesis via its C-site. (A)** Growth kinetics of sh control (non-targeting) and *ANGPTL4*-silenced (sh-1 and sh-2) A375 tumors (n = 5–6; mean ± SEM). **, P < 0.01; ****, P < 0.0001, two-way ANOVA with Bonferroni's multiple comparison test. **(B)** Representative IF images of control and *ANGPTL4*-silenced A375 primary tumor sections stained with CD31 (in green) and DAPI (in blue). Scale bar: 100 µm. **(C)** Quantitation of vascularized area in sh control (non-targeting) and *ANGPTL4*-silenced (sh-1 and sh-2) A375 primary tumors (n = 5; mean ± SD). **, P < 0.01, Mann–Whitney U test. **(D)** Growth kinetics of control, nANGPTL4-, and cANGPTL4-expressing LLC tumors (n = 7–12; mean ± SEM). ****, P < 0.0001, two-way ANOVA with Bonferroni's multiple comparison test. **(E)** Representative IF images of tumor sections from LLC co-stained with CD31 (green), Desmin (red), and DAPI (in blue). Scale bar: 100 µm. **(F)** Quantitation of vascularized area in control, nANGPTL4-, and cANGPTL4-expressing LLC primary tumors (n = 7–9; mean ± SD). ***, P < 0.001, Mann–Whitney U test.

cANGPTL4 resulted in a strong angiogenic response. In contrast, nANGPTL4 alone had no effect on vascular sprouting, but potently inhibited VEGF-A–induced sprouting angiogenesis (Fig. 4 A). To corroborate these findings in vivo, we performed mouse cornea angiogenesis assays, in which slow-release pellets of ANGPTL4, nANGPTL4, and cANGPTL4 were implanted in a cornea micropocket either alone or in the presence of VEGF-A (Fig. 4 B). Consistent with the in vitro findings, cANGPTL4 enhanced VEGF-A–induced sprouting angiogenesis, whereas nANGPTL4 significantly reduced VEGF-A–induced sprouting angiogenesis in vivo (Fig. 4, B and C; and Fig. S3 R). Taken together, the data identify cANGPTL4 as the promoter of VEGF-A–induced sprouting angiogenesis, whereas nANGPTL4 quenched the proangiogenic response of VEGF-A and thereby suppressed angiogenesis.

nANGPTL4 inhibits sprouting angiogenesis via Syndecan-4 (SDC4)

Several studies have shown that membrane-bound integrins act as cognate receptors for ANGPTL4 and cANGPTL4 (Goh et al., 2010; Huang et al., 2011; Zhu et al., 2011). Indeed, antibody-mediated blocking of integrin function reduced both ANGTL4- (Fig. S3, S and T) and cANGPTL4-stimulated sprouting angiogenesis (Fig. 4, D and E; and Fig. S3 U). However, integrin blocking did not affect nANGPTL4-mediated antiangiogenesis (Fig. 4, D and E; and Fig. S3 U), suggesting that nANGPTL4 may act via a different receptor signaling system.

Next, we investigated whether nANGPTL4 signaling was dependent on its recently identified receptor SDC4 (Kirsch et al., 2017). SDC4 is a heparan sulfate proteoglycan that controls different cellular processes like endocytosis, proliferation, and adhesion (Elfenbein and Simons, 2013). Further, loss-of-function studies in SDC4-deficient mice have identified SDC4 as the regulator of angiogenesis (De Rossi et al., 2019). We therefore transduced HUVEC with shRNAs against *SDC4* or non-targeting shRNA (control) and performed spheroid-sprouting assays in the presence or absence of nANGPTL4 (Fig. 4, F and G; and Fig. S3 V). Indeed, nANGPTL4 blunted VEGF-A–induced sprouting angiogenesis in EC transduced with control shRNA. Yet, silencing of *SDC4* in EC completely ablated the antiangiogenic

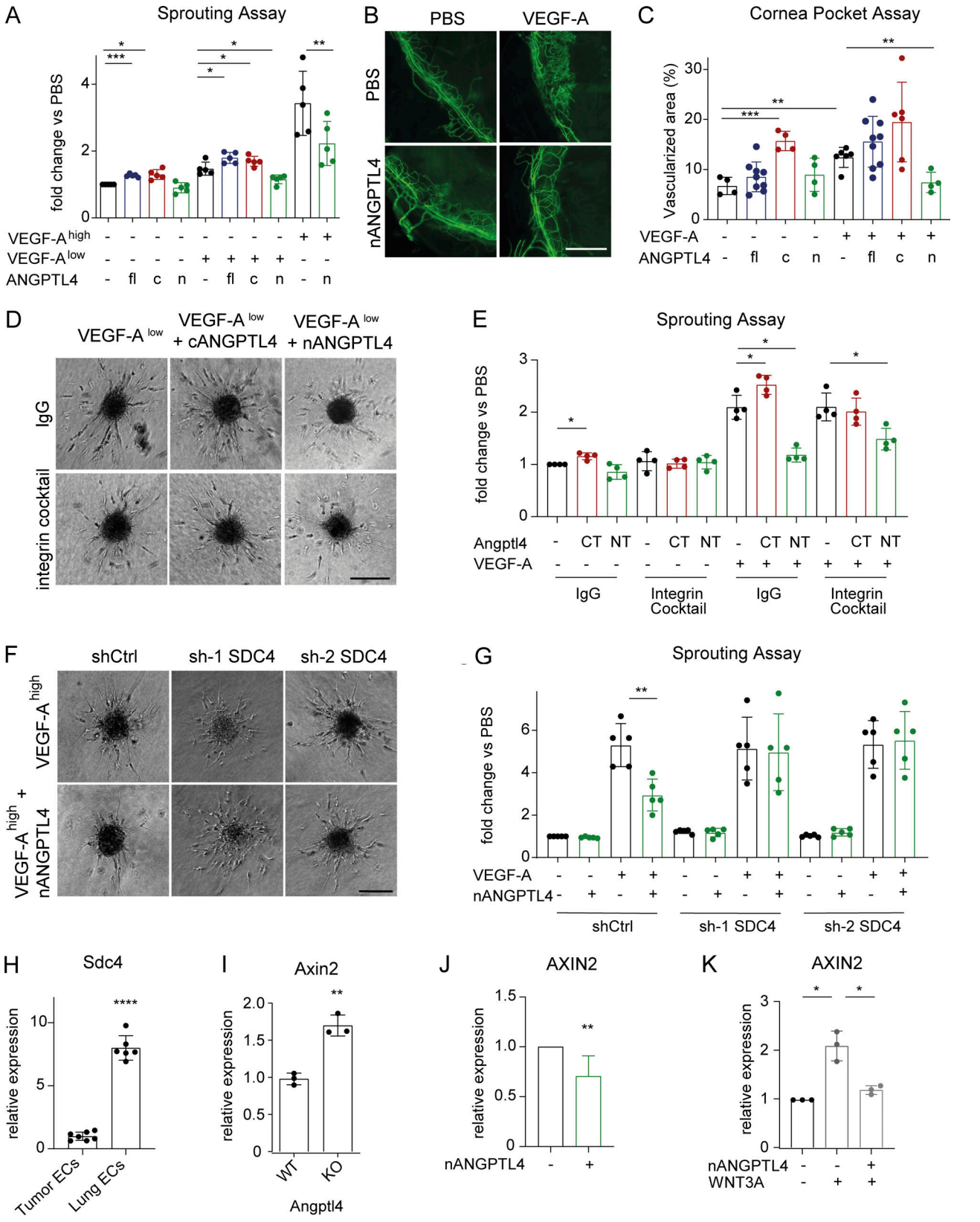

Figure 4. **nANGPTL4 and cANGPTL4 have independent and opposing functions on sprouting angiogenesis. (A)** Quantitation of the cumulative sprout length of HUVEC) spheroids stimulated with the indicated cytokines (n = 5; mean ± SD). *, P < 0.05; **, P < 0.01; ***, P < 0.001, two-tailed paired Student's t test. **(B)** Representative stitched tile scanned IF images of the corneas isolated from C57BL6/J mice stimulated with either PBS or the indicated cytokines. Corneas were stained for the EC marker CD31 (green). Scale bar: 500 µm. **(C)** Quantitation of vascularized corneal area (n = 4–9; mean ± SD). **, P < 0.01; ***, P < 0.001, unpaired Student's t test. **(D)** Representative images of IgG or integrin-blocking antibody-treated EC spheroids stimulated with the indicated

cytokines. Scale bar: 200 µm. **(E)** Quantitation of the cumulative sprout length of IgG or integrin-blocking antibody treated EC spheroids stimulated with the indicated cytokines (n = 4; mean ± SD). *, P < 0.05, paired Student's t test. **(F)** Representative images of sh control (non-targeting) and *SDC4*-silenced EC spheroids stimulated with the indicated cytokines. Scale bar: 200 µm. **(G)** Quantitation of the cumulative sprout length of EC spheroids of sh control (non-targeting) and *SDC4*-silenced EC spheroids stimulated with the indicated cytokines (n = 5; mean ± SD). **, P < 0.01, two-tailed paired Student's t test. **(H)** Quantitation of *SDC4* expression in sorted ECs from LLC primary tumors and healthy lungs (n = 6–7, mean ± SD). ****, P < 0.0001, unpaired Student's t test. **(I)** Quantitation of *Axin2* expression in whole liver lysates of WT and *Angptl4*-deficient (KO) mice (n = 3, mean ± SD). **, P < 0.01, unpaired Student's t test. **(J)** Quantitation of *AXIN2* expression by RT-qPCR in HUVEC treated with recombinant nANGPTL4 (n = 7; mean ± SD). **, P < 0.01, two-tailed paired Student's t test. **(K)** Quantitation of *AXIN2* expression by RT-qPCR in HUVEC treated with either recombinant WNT3A or a combination of WNT3A and nANGPTL4 (n = 3; mean ± SD). *, P < 0.05, paired Student's t test.

effect of nANGPTL4 (Fig. 4 G). By contrast, depletion of *SDC4* in EC did not affect both ANGPTL4- and cANGPTL4-mediated sprouting angiogenesis, suggesting that SDC4 may be a specific candidate receptor for nANGPTL4 in EC (Fig. S3, V–X). Moreover, a higher expression of *SDC4* was observed in mouse lung EC isolated from metastatic lungs as compared with primary tumor–derived EC (Fig. 4 H), indicating that nANGPTL4 has a higher probability of engaging its downstream receptor at the metastatic site.

Binding of nANGPTL4 to SDC4 was previously shown to downregulate WNT signaling resulting from the lysosomal degradation of lipoprotein receptor-related protein 6 (Kirsch et al., 2017). WNT signaling acts as a major driver for vessel formation and maturation (Franco et al., 2009; Korn et al., 2014). Indeed, the WNT target *Axin2* was found upregulated in *Angptl4*-deficient mice as compared with control mice (Fig. 4 I and Fig. S3 Y). Corroborating these results, treatment of HUVEC with recombinant nANGPTL4 resulted in transcriptional downregulation of *AXIN2* (Fig. 4 J). Moreover, treatment of HUVEC with nANGPTL4 significantly reduced WNT3A-mediated *AXIN2* upregulation (Fig. 4 K). Collectively, the data provide compelling evidence that, although cANGPTL4 enhanced sprouting by binding to integrins, nANGPTL4 reduced sprouting angiogenesis by signaling through SDC4, leading to downregulation of EC WNT signaling.

nANGPTL4 inhibits metastatic colonization

To dissect the contribution of primary tumor–derived ANGPTL4 and its cleavage fragments on metastasis, we performed systemic gain-of-function experiments by implanting control or ANGPTL4 or its cleavage fragments expressing B16F10 cells in C57BL/6J mice (Fig. 5 A). 7 d after primary tumor implantation, mice were intravenously administered WT B16F10 melanoma cells. Systemic upregulation of ANGPTL4 or nANGPTL4 significantly reduced metastasis originating from secondarily injected WT B16F10 melanoma cells (Fig. 5, B and C). In contrast, systemic upregulation of cANGPTL4 strongly promoted melanoma metastasis to the lungs (Fig. S4, A and B).

Next, we asked whether the reduction of lung metastasis upon systemic expression of ANGPTL4 was due to increased serum concentrations of ANGPTL4 or had resulted from increased concentrations of proteolytically processed ANGPTL4 fragments. Targeted mass spectrometric analysis of serum samples from mice grafted with either control or ANGPTL4-expressing tumor cells revealed that the serum nANGPTL4/ANGPTL4 ratio correlated inversely with the number of lung metastases, indicating that an increased nANGPTL4/ANGPTL4 ratio in the circulation of mice bearing ANGPTL4-expressing primary tumors was responsible for the observed antimetastatic effect in these mice (Fig. 5 D).

To validate these findings in an independent mouse model, we performed LLC postsurgical metastasis experiments, in which the primary tumors were surgically resected, making metastatic growth rate-limiting for the survival of mice (Fig. 5 E). LLC tumor cells expressing control or nANGPTL4 were subcutaneously implanted and surgically resected at approximately similar sizes (Fig. S4 C). To trace the incidence of metastasis, PET–CT (positron emission tomography/computed tomography) imaging was performed after surgical excision of primary tumors in some mice of each group (3/10; Fig. 5 F). PET–CT imaging detected metastasis as early as 2 wk after surgical resection of the primary tumor in mice implanted with control (n = 3/3)-expressing LLC tumor cells, whereas mice implanted with nANGPTL4-expressing tumor cells (n = 0/3) showed no metastatic lesions in early PET–CT evaluation. Mice implanted with nANGPTL4-expressing tumor cells had a significantly higher survival rate compared with control-implanted mice (Fig. 5 G). Conversely, mice implanted with cANGPTL4-expressing LLC had a significantly lower survival rate compared with control-implanted mice (Fig. S4, D–F). In summary, the experiments established a new paradigm, wherein two cleavage fragments of a protein have fundamentally opposing effects on metastasis: whereas nANGPTL4 suppressed metastasis formation and extended overall survival, cANGPTL4 facilitated metastasis and reduced overall survival. The antimetastatic activity of nANGPTL4 suggested that nANGPTL4 released in the circulation could act as a mediator of CTR.

To validate the potential of nANGPTL4 as an antimetastatic agent, we generated recombinant murine nANGPTL4 and assessed its therapeutic efficacy in preclinical tumor experiments (Fig. S4, G–I). Mice were preconditioned with recombinant nANGPTL4 (7 µg/injection) or PBS 2 d prior to tumor cell injection (Fig. 6 A). Thereafter, mice were intravenously injected with either PBS or recombinant nANGPTL4 twice per week for 14 d. Therapeutic administration of recombinant nANGPTL4 severely impaired melanoma lung metastasis in B16F10 and MT-RET model (Fig. 6, A–C; and Fig. S4, J–L), establishing a proof-of-principle of the antimetastatic therapeutic efficacy of recombinant nANGPTL4. Similarly, AAV-mediated systemic upregulation of nANGPTL4 reduced lung metastasis in the B16F10 model and enhanced postsurgical metastasis-free survival in the LLC model (Fig. 6, D–H; and Fig. S4, M–O). Taken together, therapeutic administration of nANGPTL4 may be a viable strategy in high-risk metastatic cancer patients.

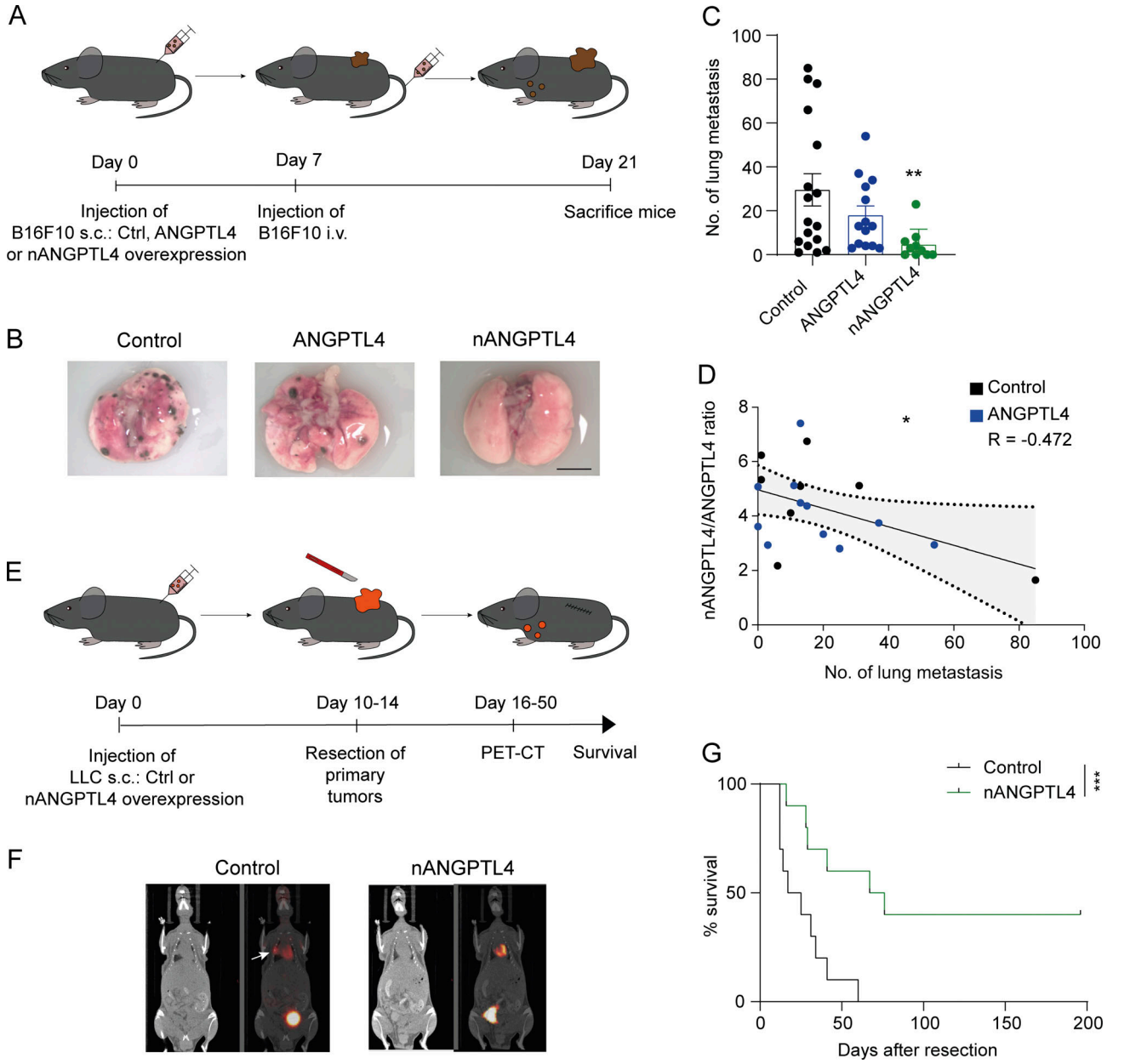

Figure 5. **nANGPTL4 inhibits metastases formation in preclinical mouse tumor models. (A)** Schematic illustration of the experimental design to investigate the effect of systemically released ANGPTL4 and nANGPTL4 on lung metastasis. **(B)** Representative images of lung metastatic foci imaged under a stereomicroscope. Scale bar: 2 mm. **(C)** Quantitation of B16F10 lung metastatic foci (n = 10–17; mean ± SEM). **, P < 0.01, Mann–Whitney U test. **(D)** Pearson correlation of nANGPTL4/ANGPTL4 ratio identified by targeted mass spectrometry in sera of control (black dots) and ANGPTL4 tumor–bearing mice (blue dots) and numbers of macroscopic metastases. The black dotted lines depict the 95% confidence interval of the regression line (n = 19, r = −0.4725). *, P < 0.05, Pearson correlation. **(E)** Schematic representation of the LLC postsurgical metastasis model. **(F)** Representative PET–CT images, 2 wk after tumor resection in mice implanted with control or nANGPTL4-expressing LLC. **(G)** Kaplan–Meier plot showing the percentage survival of mice implanted with control or nANGPTL4-expressing LLC tumor cells following primary tumor resection (n = 10). ***, P < 0.001, log-rank (Mantel–Cox) test.

To discern the mechanism of nANGPTL4 inhibitory effects on metastasis, we conducted genome-wide RNA sequencing (RNAseq) on control and nANGPTL4 AAV-treated lung EC. In line with the in vitro findings, gene set enrichment analysis (GSEA) unveiled that pathways regulating angiogenesis and WNT signaling were downregulated upon nANGPTL4 treatment (Fig. S5, A–C). Immunofluorescence-based quantification of the vascular marker CD31 and the activated form of β-catenin, a master transcription factor of WNT signaling in EC of the primary tumor and metastatic site, displayed potent inhibition of WNT signaling and CD31 expression at the metastatic site in nANGPTL4-treated mice (Fig. S5, D–G). In contrast, WNT signaling and CD31 levels were not altered at the primary tumor site (Fig. S5, H–J). The data indicate that nANGPTL4 exerts its antimetastatic functions by suppressing WNT signaling and reducing vascularity at the metastatic site.

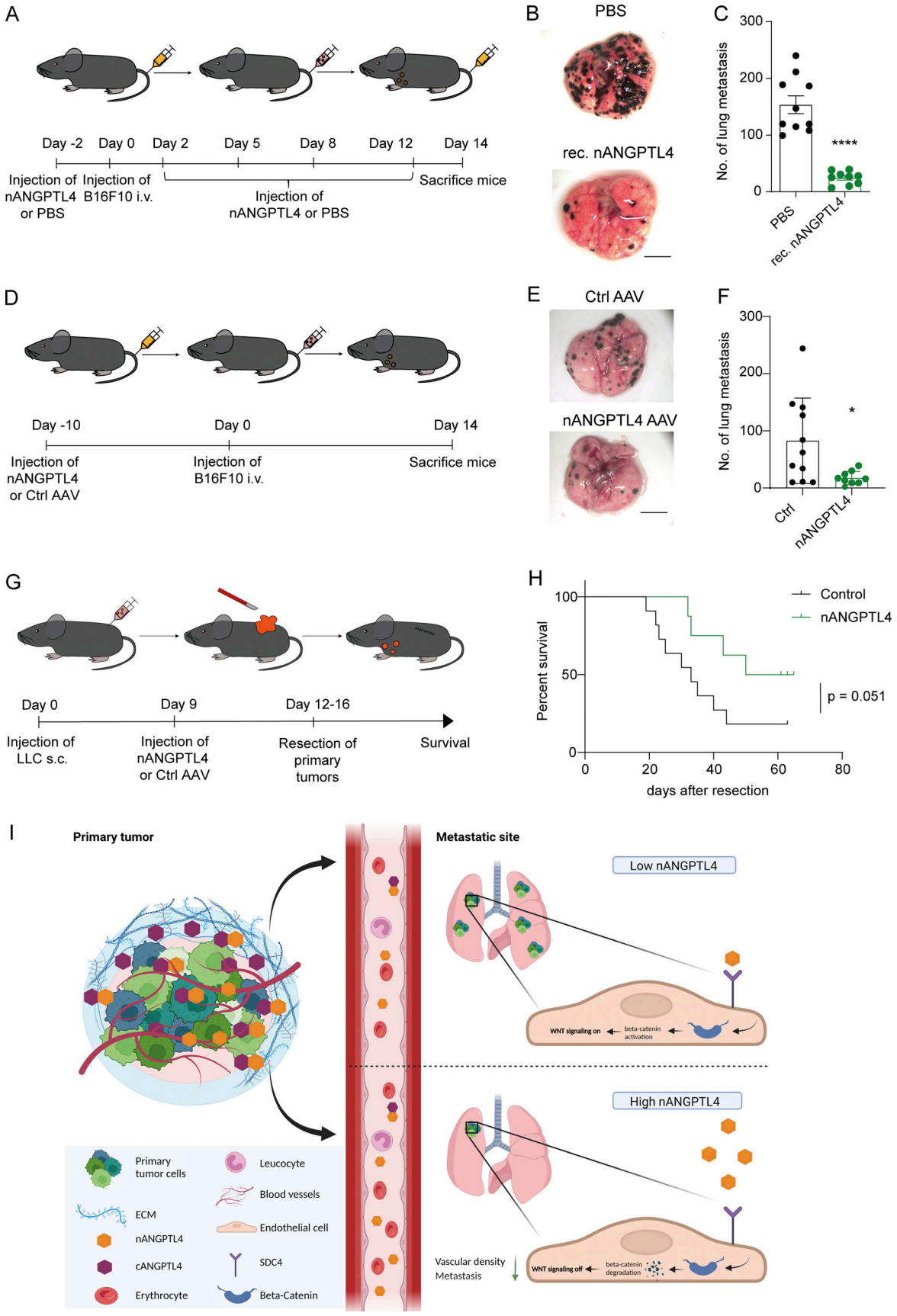

Figure 6. **Therapeutic administration of nANGPTL4 inhibits metastasis formation. (A)** Schematic representation of the experimental metastasis model to evaluate the therapeutic efficacy of recombinant nANGPTL4. Mice were injected with either recombinant nANGPTL4 (7 µg/shot) or PBS as depicted in the

scheme. **(B)** Representative images of metastatic lung foci from mice treated with PBS or nANGPTL4. Scale bar: 2 mm. **(C)** Graph representing the quantitation of metastatic foci (n = 9–10; mean ± SEM). ****, P < 0.0001, Mann–Whitney U test. **(D)** Schematic representation of the experimental metastasis model to evaluate the therapeutic efficacy of nANGPTL4 AAV. Mice were injected with 10^{11} nANGPTL4 or control AAV. **(E)** Representative images of metastatic lung foci from mice treated with control or nANGPTL4 AAV. Scale bar: 2 mm. **(F)** Graph representing the quantitation of metastatic foci (n = 9–11; mean ± SD). *, P < 0.05, Mann–Whitney U test. **(G)** Schematic representation of the LLC postsurgical metastasis model. **(H)** Kaplan–Meier plot showing the percentage survival of control or nANGPTL4 AAV-injected mice implanted with LLC tumor cells following primary tumor resection (n = 8–11). Log-rank (Mantel–Cox) test. **(I)** Graphical abstract illustrating the differential function of cANGPTL4 and nANGPTL4 in the primary tumor and at the metastatic site.

Discussion

Surgical removal of a primary tumor continues to be the gold standard treatment for solid tumors and often results in significant improvement in overall survival (Chiarella et al., 2012; Tohme et al., 2017). However, excision of the primary tumor alters the cancer patient's systemic homeostasis, which may affect hitherto dormant metastatic cells (Krall et al., 2018). CTR, a phenomenon by which systemically acting signals from the primary tumor may control the growth of secondary tumors, may explain the social crosstalk of a primary tumor and distant site metastases as a roadblock for the growth of secondary metastasis (Chiarella et al., 2012). The comprehensive understanding of CTR will not only shed mechanistic insight into the complexity of the metastatic cascade but may also lead to the identification of novel therapeutic targets.

This study was aimed at deciphering the conflicting reports portraying ANGPTL4 either as a proangiogenic and protumorigenic molecule (Baba et al., 2017; Chen et al., 2018; Hu et al., 2016; Huang et al., 2011; Izraely et al., 2017; Kolb et al., 2019; Le Jan et al., 2003; Li et al., 2011; Li et al., 2015; Liao et al., 2017; Ma et al., 2010; Padua et al., 2008; Tian et al., 2009; Zhang et al., 2018; Zhu et al., 2011) or as a primarily antiangiogenic (Cazes et al., 2006; Galaup et al., 2012; Gomez Perdiguero et al., 2016) and antitumorigenic cytokine (Galaup et al., 2006; Ng et al., 2014; Okochi-Takada et al., 2014). The results of this study have shed unprecedented insights into the mechanisms of CTR and identified nANGPTL4 as a primary tumor–derived inhibitor of metastasis with potential as a therapeutic target. We identified ANGPTL4 and its cleavage fragments as crucial players in sustaining CTR. The N- and C-terminal fragments of ANGPTL4 were found to exert distinctly opposing functions during tumor progression. cANGPTL4 enhanced sprouting angiogenesis by binding to integrins to promote primary tumor growth and metastatic progression in a postsurgical metastasis model. In contrast, nANGPTL4 interacted with EC-expressed SDC4, leading to a reduction in WNT signaling and inhibition of sprouting angiogenesis. Moreover, nANGPTL4 significantly enhanced overall survival in a postsurgical metastasis model, and therapeutic treatment with recombinant nANGPTL4 profoundly suppressed lung metastasis (Fig. 6 I).

Several clinical biomarker studies have shown that ANGPTL4 levels correlate with primary tumor growth and metastasis development in different types of cancers. Yet, these studies had presumably detected ANGPTL4 (Le Jan et al., 2003; Nakayama et al., 2010; Nakayama et al., 2011; Shibata et al., 2010; Wang et al., 2010). Fully in concordance with these previous reports, we show in the present study that ANGPTL4 increased with malignancy in colon cancer and melanoma patient tissue samples. Yet, by employing N- and C-specific ANGPTL4 antibodies, we could trace the spatial localization of ANGPTL4 and its cleavage fragments in indexed serum samples and primary tumor tissue biopsies. While uncleaved ANGPTL4 was mainly localized in the local primary tumor tissues, nANGPTL4 was predominately present in systemic circulation. Moreover, reduced systemic nANGPTL4 expression was observed in end-stage metastasis patients, validating our preclinical findings that circulating nANGPTL4 may in fact prevent the outgrowth of metastases.

The findings of the present study also reconcile the extensively reported conflicting protumorigenic and antitumorigenic functions of ANGPTL4. Fully in-line with the findings reported here, studies characterizing ANGPTL4 as a protumorigenic molecule essentially all manipulated ANGPTL4 expression locally in the tumor microenvironment (Baba et al., 2017; Chen et al., 2018; Hu et al., 2016; Huang et al., 2011; Izraely et al., 2017; Kolb et al., 2019; Le Jan et al., 2003; Li et al., 2011; Li et al., 2015; Liao et al., 2017; Ma et al., 2010; Padua et al., 2008; Tian et al., 2009; Zhang et al., 2018; Zhu et al., 2011). Accordingly, silencing or inhibition of tumor-derived ANGPTL4 restricted tumor growth and reduced angiogenesis, whereas local expression of cANGPTL4 enhanced tumor growth and angiogenesis. Expression of cANGPTL4 also increased metastasis and reduced postsurgical survival in mice. In contrast, in reports in which ANGPTL4 was altered systemically, upregulation of ANGPTL4 led to an antiangiogenic and antitumorigenic effect, which, according to the findings of this study, may have resulted from proteolytic liberation of systemically acting nANGPTL4 (Cazes et al., 2006; Galaup et al., 2006; Galaup et al., 2012; Gomez Perdiguero et al., 2016; Ito et al., 2003; Ng et al., 2014; Okochi-Takada et al., 2014). Indeed, systemically released nANGPTL4 inhibited angiogenesis, reduced metastasis, and prolonged overall survival of mice in this study.

Proteolytic cleavage of ANGPTL4 was identified in this study as the mechanism responsible for liberating the cryptic antiangiogenic and antimetastatic activity residing within ANGPTL4. Furin proprotein convertases have been shown to cleave ANGPTL4 (Lei et al., 2011; Tan et al., 2012). Yet, these are ubiquitously expressed, and we have so far not been able to unambiguously identify the site of ANGPTL4 cleavage within the body. Attempts to correlate furin proprotein convertase expression with the tracing of the ANGPTL4 fragments in human tumors were not conclusive. We therefore hypothesize that ANGPTL4 may not be cleaved locally in the tumor tissue, but rather in circulation or in the liver. This hypothesis is also supported by earlier findings showing that incubation of ANGPTL4 with serum induces its cleavage (Ge et al., 2004). In turn, the preferential detection of nANGPTL4 and the almost complete absence of circulating cANGPTL4 may result from the

selective sequestration of cANGPTL4 from circulation. ANGPTL4 has been shown to bind to the extracellular matrix via its C-site (Goh et al., 2010). The extracellular matrix could thereby sequester ANGPTL4 and cANGPTL4 and serve as a local reservoir for these protumorigenic forms of ANGPTL4, as, for example, has also been shown for fibroblast growth factors (Vlodavsky et al., 1987).

Several endogenous inhibitors of angiogenesis have been discovered, and clinical trials were initiated for a few of them (Rong et al., 2012; Westphal, 2004). Yet, the translational exploitation of such endogenous inhibitors has so far not yielded sustainable success in the clinic. Here, we report the potent antiangiogenic and antimetastatic activity of recombinant nANGPTL4. Therapeutic administration of nANGPTL4 significantly impeded the formation of lung metastases. Interestingly, nANGPTL4 has been reported to inhibit the activity of LPL. Potential side effects of long-term nANGPTL4 treatment could consequently be coronary artery disease or diabetes resulting from increased concentrations of serum triglycerides (Dijk and Kersten, 2014). However, it may be possible to avoid such potential side effects by introducing the E40K mutation into nANGPTL4. This mutation within nANGPTL4, which is present in ∼4% of the population with European ancestry, significantly reduces the activity of ANGPTL4 to inactivate LPL, resulting in reduced plasma triglyceride levels (Dewey et al., 2016). Future studies will be required to assess the clinical safety and efficacy of recombinant WT and mutated nANGPTL4.

In conclusion, by employing multiple preclinical tumor models in combination with manipulatory in vivo and in vitro experiments, the present study has shed ground-breaking insights into the mechanisms of CTR to establish opposing protumorigenic and antitumorigenic functions of ANGPTL4 and cANGPTL4 compared with nANGPTL4, respectively. Corresponding human clinical biomarker analyses substantiated the ANGPTL4 CTR paradigm in human tumors. The antiangiogenic and antimetastatic functions of recombinant nANGPTL4 deserve further translational exploitation.

Materials and methods

Patient samples and ethical approval

Tumor tissue samples were provided by the tissue bank of the National Center for Tumor Diseases (Heidelberg, Germany) in accordance with the regulations of the tissue bank and the approval of the Ethics Committee of Heidelberg University.

Fresh frozen melanoma and lung tumor samples, serum samples and paraffin-embedded melanoma, SCC, and actinic keratosis (AK) samples (TMAs) were provided by the University Medical Centre Mannheim. The study was approved by the Ethical Committee of Heidelberg University (2010-318N-MA and 2014-835R-MA). Informed written consent was obtained from all participants and they agreed to use their samples for research and to publish the acquired data in accordance with the Helsinki principles for the enrolment in research protocols.

Normal tissue, lung cancer, and colon cancer TMAs were purchased from Abcam (ab178228, ab178186, and ab178094).

Patient classification and serum collection

A certified, interdisciplinary tumor board (dermatology, ear, nose, and throat, general surgery, radiology, nuclear medicine, and neurosurgery) classified the patients based on serum parameters (S100A4, LDH) and radiological examination (using the internationally accepted RECIST 1.1 criteria). A patient was characterized with a stable disease when there was neither sufficient increase nor decrease in their tumor burden (growth of pre-existing metastasis or occurrence of new metastasis) compared with the previous measurements. In contrast, a patient with an increase in tumor burden compared with the previous measurement was considered to have a progressive disease. The serum levels of nANGPTL4 were determined from samples collected 1 wk before the tumor board meeting.

Cell culture

LLC, B16F10, HEK293T, and 4T1 were obtained from the American Type Culture Collection. All human melanoma cells (SK-MEL-17, HT-144, MeWo, SK-MEL-10, SK-MEL-28, C32, WM266-4, A375, MZ-7-MEL, Mel-501, and SK-MEL-23) and human SCC cell lines (HaCaT-24, Scl-24, Met-1, Met-M2, Met4, and RT-375) were kindly provided by J.S. Utikal and P. Boukamp (IUF-Leibniz Research Institute for Environmental Medicine, Düsseldorf, Germany), respectively. All cancer cells were cultured in DMEM high glucose (Gibco) supplemented with 10% FCS and 1% penicillin/streptomycin (Sigma-Aldrich). Human umbilical vein ECs (HUVEC; Promocell) were cultured in Endopan-3 medium supplemented with growth factors (PAN Biotech GmbH). All cells were cultured at 37°C and 5% CO_2 and routinely tested for mycoplasma by PCR.

RNA isolation, cDNA synthesis, and RT-qPCR

RNA was isolated using GenElute Mammalian Total RNA Purification Kit (cat. no. RTN350; Sigma-Aldrich) according to the manufacturer's instructions. cDNA synthesis from isolated RNA was done using QuantiTect Reverse Transcription Kit (Qiagen) according to the manufacturer's instructions. Synthesized cDNA was used to perform RT-qPCR by using TaqMan Fast Advanced Mastermix (cat. no. 4444557; Life Technologies) and TaqMan probes (Applied Biosystems) or SYBR Green-based qPCR was performed with Power SYBR Green PCR Master Mix (Thermo Fisher Scientific) on an Applied Biosystems StepOnePlus cycler. TaqMan probes used were *SCD4*: Hs01120908_m1; *ANGPTL4*: Hs01101123_g1; *AXIN2*: Hs00610344_m1; *RNS18S*: Hs03928985_g1; *Axin2*: Mm00443610_m1; *Sdc4*: Mm00488527_m1; and *Actb*: Mm00607939_s1. All the TaqMan probes were purchased from Thermo Fisher Scientific. Gene expression levels were analyzed based on the ΔΔCt relative quantification method.

Immunofluorescence staining of ANGPTL4 in human TMAs

Tissue sections (4 µm) were obtained from formalin-fixed paraffin-embedded TMA tissue blocks. Tissue sections were dried on super frost slides overnight at 37°C. The sections were then deparaffinized in HistoClear and rehydrated in decreasing concentrations of ethanol. Antigen retrieval was done using Proteinase K, and slides were incubated for 10 min at 37°C. Sections were then blocked in 5% BSA and 10% normal goat

serum in PBS for 1 h, followed by overnight incubation with the respective primary antibody at 4°C. Following primary antibody incubation, the sections were washed and incubated with the secondary antibody for 1 h at room temperature.

For mouse tissues, tissue samples were embedded in Tissue-Tek OCT on dry ice. Cryosections (7 µm) were cut and fixed in ice-cold methanol for 20 min at −20°C. Sections were then blocked in 10% ready-to-use normal goat serum (Life Technologies) for 1 h, followed by overnight incubation with the respective primary antibody at 4°C. Following primary antibody incubation, the sections were washed and incubated with the secondary antibody for 1 h at room temperature. For immunofluorescence on mouse tissues, the following antibodies were used: rat anti-CD31 (cat. no. 550300; BD Bioscience), rabbit anti-Desmin (cat. no. Ab15200-1; Abcam), and β-catenin (cat. no. 8814; Cell Signaling). The secondary anti-rat A488 and anti-rabbit A546 (Life Technologies) were used. Nuclei were stained with Hoechst (cat. no. H1399; Invitrogen). Images were acquired using Zeiss Axio Scan, and image analysis was performed with Fiji.

Immunohistochemistry stainings of ANGPTL4 in human TMAs

Tissue sections (4 µm) were obtained from formalin-fixed paraffin-embedded TMA tissue blocks. Tissue sections were dried on super frost slides overnight at 37°C. Staining was done as described previously (Shafik et al., 2015). In brief, the tissue sections were deparaffinized, rehydrated, and incubated in 3% H_2O_2 for 10 min. For antigen retrieval, specimens were heated for 20 min in 10 mmol/l citrate buffer (pH 6.0) in a microwave oven (700 W). Slides were incubated with mouse monoclonal to ANGPTL4 (1:150, cat. no. MAB019Ra21; Life Science Inc.) overnight at room temperature. Following primary antibody incubation, antibody binding was detected using the DAB$^+$ substrate Chromogen System (Dako Omnis) according to the manufacturer's recommendations. Color development was performed with 3,3′-diaminobenzidine and counterstained with hematoxylin. Pictures were acquired using Zeiss Axio Scan, and image analysis was done with Fiji.

Western blotting of human tumor tissues and human serum

Human tumor tissues were lysed in radioimmunoprecipitation assay buffer, and the protein lysates were separated on 12% SDS-PAGE gels. Serum samples were directly loaded on 12% SDS-PAGE gels (0.4 µl/lane). Proteins were transferred onto a methanol-activated polyvinylidene fluoride membrane and blocked with 5% milk in PBS with Tween 20 for 1 h. After blocking, the membranes were incubated overnight at 4°C with the following primary antibodies: cANGPTL4 (ab115798; Abcam), nANGPTL4 (Mandard et al., 2004), and Transferrin (PA3-913; Thermo Fisher Scientific) and then diluted 1:1,000 in PBS with Tween 20 containing 5% milk powder at 4°C overnight. Following primary antibody incubation, the membranes were washed and incubated with specific secondary horseradish peroxidase-conjugated antibodies (anti-rabbit HRP, DakoCytomation, P0448) for 1 h at room temperature. Proteins were detected with enhanced chemiluminescence (Pierce) and viewed using Amersham Imager 600 (GE). Densiometric analysis was performed using Fiji.

Proteome profiling of ANGPTL4 by targeted liquid chromatography–mass spectrometry

Elutes from immunoprecipitated ANGPTL4 were reduced, alkylated, and digested with trypsin. After adding N- and C-term–specific heavy-labeled reference peptides (JPT.com) to the samples at 5 fmol/µg of total protein, peptide standards were, together with their endogenous counterparts, specifically monitored using liquid chromatography–mass spectrometry and parallel-reaction monitoring. Acquired data were analyzed using Skyline software V2.1 (https://skyline.ms/project/home/software/Skyline/begin.view). The mass spectrometry data files have been deposited to the PRIDE database under the accession number PXD020269.

Lentiviral production and transduction

Lentivirus was produced by transfecting HEK 293T cells with lentiviral construct of interest (21 µg), envelope plasmid pMD2.G (14 µg), and packaging plasmid psPAX2 (21 µg) using polyethylenimine solution (cat. no. 408727; Sigma-Aldrich). Lentiviral supernatants were harvested twice: 48 and 72 h after transfection. The collected supernatant was filtered through a 0.45-µm filter and centrifuged at 800,000 *g* for 2 h at 4°C. The resulting lentiviral pellet was dissolved in PBS. A375 cells were transduced with lentiviral particles expressing shRNA constructs (Dharmacon): non-targeting (RHS4346), sh-1 *ANGPTL4* (VGH5518_200243106), and sh-2 *ANGPTL4* (VGH5518_200298879). HUVEC were transduced with lentiviral particles expressing shRNA constructs (Dharmacon): non-targeting (RHS4346), sh-1 *SDC4* (V3LHS_411904), and sh-2 *SDC4* (V2LHS_30982). LLC and B16F10 cells were transduced with lentivirus to express either fl, n, c ANGPTL4, or control Plenti vector (cat. no. V496-10; Invitrogen). In front of the CDS of cANGPTL4, a secretion sequence was added to generate a secretable form of cANGPTL4.

Cloning, expression, and purification of ANGPTL4 proteins

The sequences encoding mouse ANGPTL4-NT (amino acids 24–164) and mouse ANGPTL4-CT (amino acids 169–410) were cloned into the pACEBac1-EGT vector (EMBL). Each coding sequence was followed by an HRV 3C protease cleavage site and a C-terminal StrepIItag. These constructs were used for transposition in *Escherichia coli* DH10EMBacY cells, and the isolated bacmid DNAs were then utilized to generate recombinant baculovirus. For protein expression, 5 ml of baculovirus was added to 0.5 liter of Hi5 cells at a density of 1×10^6 cells/ml. The infected Hi5 cells were grown for 48 h in Sf-900 III SFM medium (Thermo Fischer Scientific) at 27°C. Cells were harvested by centrifugation. The cell pellet was discarded, and the cell culture medium was mixed carefully with 50 ml of a buffer containing 1 M Tris pH 8.0, 1.5 M NaCl, 10 mM EDTA, and 1.2 ml BioLock solution (IBA). The mixture was gently stirred on ice for 15 min and filtered over a sterile 22-µm Steritop bottle top filter (Merck Millipore). The resulting supernatant was loaded onto a 1-ml StrepTactinXT Superflow high capacity column (IBA) pre-equilibrated with running buffer (100 mM Tris pH 8.0, 150 mM NaCl, 1 mM EDTA). After loading, the column was washed with running buffer and eluted with running buffer supplemented with 50 mM biotin. The elution fractions

containing either mANGPTL4-NT or mANGPTL4-CT were pooled and dialyzed overnight at 4°C against a storage buffer (50 mM Na phosphate pH 7.2, 150 mM NaCl).

EdU cell proliferation assay

Proliferation assays of B16F10, LLC, and A375 were performed using the Click-iT EdU Alexa Fluor 647 Flow Cytometry Assay Kit (cat. no. C10419; Life Technologies). For each cell line, 300,000 cells were seeded per 6-well and allowed to adhere for 24 h. Subsequently, cells were serum-starved for 3 h and then pulsed with EdU (10 μM) for 3 h. Next, the cells were harvested and fixed for 15 min with Click-iT fixative solution. Permeabilization was performed in saponin-based permeabilization buffer for 15 min. EdU^+ cells were detected by incubating cells with Click iT detection cocktail for 30 min followed by analysis with a BD FACSCanto II flow cytometer. The percentage of EdU^+ cells was determined with the FlowJo software.

Survival analysis

Overall survival analysis of TCGA gene expression datasets from 32 tumor entities was performed using the GEPIA-2 web portal. The following tumors were used for analysis adrenocortical carcinoma, bladder urothelial carcinoma, breast invasive carcinoma, cervical SCC, and endocervical adenocarcinoma, cholangiocarcinoma, colon adenocarcinoma, lymphoid neoplasm diffuse large B cell lymphoma, esophageal carcinoma, glioblastoma multiforme, head and neck SCC, kidney chromophobe, kidney renal clear cell carcinoma, kidney renal papillary cell carcinoma, acute myeloid leukemia, brain lower grade glioma, liver hepatocellular carcinoma, lung adenocarcinoma, lung SCC, mesothelioma, ovarian serous cystadenocarcinoma, pancreatic adenocarcinoma, pheochromocytoma and paraganglioma, prostate adenocarcinoma, rectum adenocarcinoma, sarcoma, skin cutaneous melanoma, stomach adenocarcinoma, testicular germ cell tumors, thyroid carcinoma, uterine corpus endometrial carcinoma, uterine carcinosarcoma, and uveal melanoma. Kaplan–Meier plots were generated by comparing high (>75 percentile) and low (<25 percentile) gene expression of 38 angiogenic molecules with the overall survival of patients.

In vivo tumor studies

Male C57BL/6J (WT) or CB17-SCID mice (8–10 wk old) were purchased from Charles River. *Angptl4*$^{-/-}$ were kindly provided by S. Kersten. All mice were housed in a 12-h light/dark cycle with free access to food and drinking water in specific pathogen–free animal facilities. All animal experiments were approved by the governmental Animal Care and Use Committees (permits: DKFZ305, G23/16, G171/16, G257/18, G286/18, G163/16, G254/18, and G101/20 from Regierungspräsidium Karlsruhe, Germany).

A375 melanoma experiments

For primary tumor experiments, CB17-SCID mice were subcutaneously injected in the flank region with 10^6 parental or *ANGPTL4* knockdown A375 melanoma cells. At a tumor size of 500 mm^3, mice were euthanized, and tumors and blood samples were acquired for further processing. The tumor volume was calculated using the formula (length × breadth × height)/2.

LLC lung cancer primary tumor experiments

Cells expressing *Angptl4* cleavage fragments (nANGPTL4, cANGPTL4) or control LLC (10^6 in PBS) were inoculated subcutaneously in C57BL/6J mice. At a tumor size of 300 mm^3, mice were euthanized, and tumors and blood samples were acquired for further processing.

B16F10 melanoma primary tumor experiments

Male C57BL/6J (WT) mice (8–10 wk old) were subcutaneously injected in the flank region with 10^6 B16F10 cells expressing *Angptl4* cleavage fragments (nANGPTL4, cANGPTL4) or control plasmid. At a tumor size of 1,000 mm^3, mice were euthanized, and tumors and blood samples were acquired for further processing.

B16F10 melanoma combined primary and metastatic tumor experiments

Cells expressing *Angptl4* or its cleavage fragments (nANGPTL4, cANGPTL4) or control B16F10 (10^6 in PBS) were inoculated subcutaneously in C57BL/6J mice. After 7 d, B16F10 cells (2.5×10^5 in PBS) were injected into the tail vein. After 2 wk, lungs were collected and melanoma metastatic foci were counted.

LLC lung cancer metastases experiments

Cells expressing *Angptl4* cleavage fragments (nANGPTL4, cANGPTL4) or control LLC (10^6 in PBS) were inoculated subcutaneously in C57BL/6J mice. Primary tumors were surgically resected at an average size of 250–450 mm^3. The mice were routinely checked for the experimental endpoint criteria after resection.

Therapeutic administration of nANGPTL4

C57BL/6J mice were pretreated with one shot of either nANGPTL4 protein or PBS intravenously. 2 d later, 2.5×10^5 B16F10 or MT-RET cells were intravenously injected. Mice were administered thereafter with nANGPTL4 protein or PBS intravenously twice a week. 2 wk later, lungs were collected and melanoma metastatic foci were counted.

Administration of nANGPTL4-overexpressing AAV

C57BL/6J mice were intravenously injected with 10^{11} viral particles of control or nANGPTL4 AAV. 10 d later, 2.5×10^5 B16F10 cells were intravenously injected. 2 wk later, lungs were collected and melanoma metastatic foci were counted. In the LLC resection model, 10^6 LLCs were inoculated subcutaneously in C57BL/6J mice. 9 d after tumor cell injection, 10^{11} viral particles of control or nANGPTL4 AAVs were injected intravenously. Primary tumors were surgically resected at an average size of 250–450 mm^3. The mice were routinely checked for the experimental endpoint criteria after resection.

Mouse lung and primary tumor EC isolation

Mouse lungs and primary tumors were enzymatically digested in a 5 ml solution containing 4 mg/ml liberase and 10 μg/ml Dnase1 in DMEM high glucose media at 37°C for 30 min. Tissue lysates were passed through 19-G cannula syringes and further filtered through 100-μM filters. To lyse erythrocytes, the tissue

lysates were incubated with ammonium chloride potassium lysis buffer for 5 min, and the cell suspension was subsequently washed with PBS/3% FCS. Next, positive selection using CD31 microbeads (cat. no. 130-097-418; Miltenyi Biotec) was performed to enrich the EC according to the manufacturer's protocol. ECs were further FACS-sorted for the surface marker profile $CD45^-/LYVE1^-/PDPN^-/TER\text{-}119^-/CD31^+$ using the following antibodies: CD45 FITC (cat. no. 553775; BD Pharmingen), CD31 APC (cat. no. 551262; BD Pharmingen), PDPN Alexa 488 (cat. no. 53-5381-82; eBioscience), TER-119 FITC (cat. no. 561032; BD Pharmingen), and LYVE1 Alexa 488 (cat. no. 53-0443-82; eBioscience).

RNAseq

Total RNA was isolated from control and nANGTPL4 AAV-treated lung EC using an Arcturus PicoPure RNA isolation kit (Thermo Fisher Scientific) according to the manufacturer's protocol. The sequencing libraries were prepared using SMARTer Ultra Low RNA v4 Kit (Clontech) with 10 ng of base material and sequenced on Novaseq 6000 S1 (50-bp paired-end). The RNAseq data were processed and aligned using DKFZ OTP RNAseq workflow (Reisinger et al., 2017). Differential gene expressionfiler 4.0 (Love et al., 2014; Wu et al., 2021). The raw RNAseq data have been deposited under the GEO accession no. GSE210291.

Spheroid sprouting assay in vitro

HUVEC (2×20^4) were suspended in 20% Methocel/80% EGM solution and plated in 25-µl droplets on a squared petri dish and incubated upside down at 37°C. Next, spheroids were harvested in PBS + 10% FCS and resuspended in a mixture of 80% Methocel and 20% FCS. 500 µl of a collagen mix was added to the spheroids (62.5 µl Medium 199, 0.5 ml collagen, 6 µl 2 M NaOH, 50 µl HEPES buffer). Subsequently, equal volumes of the collagen-spheroid mix were added to a 24-well plate, and the gels were polymerized for 30 min at 37°C. The spheroids were treated with the following recombinant proteins: 10 ng of VEGF-A (VEGF-A high, R&D, 293-VE), 1 ng of VEGF-A (VEGF-A low), and 400 ng of NT- (8249-AN; R&D), CT- (3485-AN; R&D), or FL-ANGPTL4 (4487-AN; R&D) for 24 h. For sprouting assays with integrin-blocking antibodies, gels were incubated with 2 µg of each integrin-blocking antibody or mouse IgG for 1 h prior to the addition of recombinant proteins. After stimulation, gels were fixed by adding 1 ml Histofix. Images were taken using Olympus IX-81 microscope, and the cumulative sprout length was determined using Cell P software. 10 spheroids were analyzed for each experimental condition.

Aortic ring assay ex vivo

Angiogenic sprouts were evaluated from thoracic aortas as previously described (Baker et al., 2011). In brief, aortas were dissected from cervically dislocated 8- to 12-wk-old male C57BL/6 mice (Charles River) and sliced into 0.5-mm sections and incubated overnight in serum-free OptiMEM (cat. no. 51985-026; Gibco) at 37°C. Aortic rings were embedded in 1× DMEM containing type I collagen (cat. no. 08–115; 1 mg/ml; Millipore). Aortic rings were supplemented with OptiMEM (2.5% FCS) containing the following recombinant proteins: 3.13 ng/ml for low VEGF-A (cat. no. 293-VE; R&D Systems), 50 ng/ml for high VEGF-A, 400 ng/ml ANGPTL4 (cat. no. 4487-AN-050; R&D Systems) or PBS and incubated at 37°C. After 7 d of incubation, the average number of sprouts was counted manually under a phase-contrast microscope. For staining, the aortic rings were fixed in 4% formalin for 30 min at room temperature. Aortic rings were then blocked in PBS containing 10% FCS for 30 min at 37°C followed by overnight incubation with BS1-lectin FITC (cat. no. L9381/L5264; Sigma-Aldrich) at 4°C. Images were acquired using a confocal microscope (Leica Sp5).

Cornea pocket assay

A partial incision was made in the mid-cornea using a 30° microknife on anesthetized male C57BL/6J mice. A von Graefe knife was inserted under the edge of the inferior lip of the partial incision to create a pocket and lengthen it toward the inferior limbus. Equal size slow-release pellets were prepared by mixing appropriate amounts of growth factor with 5 µl Hydron (12% poly [2-hydroxyethyl methacrylate] [cat. no. P3932-10 G]/99.5% ethanol) and 1 µl 10% sucralfate solution (in PBS). Pellets (0.4 × 0.4 mm) were implanted into the pocket at 1.0 ± 0.2 mm distance from the corneal limbus, as previously described (Tang et al., 2011). The following pellets were prepared: 200 ng (ANGPTL4 [cat. no. 4487-AN-050], cANGPTL4 [cat. no. 3485-AN-050], and nANGPTL4 [cat. no. 8249-AN-050]), and 160 ng (VEGF-A). The mice were sacrificed after 7 d, and the corneas were isolated. Corneas were fixed in cold methanol for 10 min, washed with PBS+0.3% Triton for permeabilization, and stained with anti-CD31 antibody (cat. no. 550300; BD Bioscience). Images were taken with Zeiss Axio Scan and analyzed with Fiji.

Quantitation and statistical analysis

All data are expressed as mean with error bars depicted as SD or SEM (indicated in figure legends). *n* represents the number of independent experiments in the case of in vitro experiments and the number of mice for in vivo experiments. Statistical analyses were performed using GraphPad Prism 6 and 7. Comparisons between two groups were made using two-tailed unpaired Student's *t* test, non-parametric Mann–Whitney *U* test, two-way ANOVA, log-rank (Mantel–Cox) test, or paired *t* test. A P value of <0.05 was considered statistically significant.

Online supplemental material

Fig. S1 shows the overall survival analysis of key angiogenic molecules in 32 tumor entities. Fig. S2 characterizes the functional role of ANGPTL4 in clinical and preclinical settings. Fig. S3 shows the differential functions of ANGPTL4 and its cleavage fragments. Fig. S4 shows that the proteolytically cleaved fragments of ANGPTL4 differentially regulate metastasis. Fig. S5 shows that nANGPTL4 perturbs angiogenesis and WNT signaling at the metastatic site. Table S1 illustrates the clinicopathological data of the patients included in this study.

Data availability

The mass spectrometry data files have been deposited to the PRIDE database under the accession number PXD020269. The

raw RNA sequencing data has been deposited under the GEO accession no. GSE210291.

Acknowledgments

We would like to thank Dr. Damir Krunic (Imaging Core Facility of the German Cancer Research Center [Deutsches Krebsforschungszentrum; DKFZ] Germany) for assistance in image analysis. We thank the tissue bank of the National Center for Tumor Disease (NCT Heidelberg, Germany) for providing TMAs and for assisting in the staining of TMAs. We thank Yvonne Nowak (Skin Cancer Unit DKFZ; Germany) and Julia Flock (Protein Expression and Purification Core Facility; European Molecular Biology Laboratory, Germany) for their excellent technical support. The DKFZ flow cytometry, light microscopy, genomics and proteomics, omics IT and data management core facility, and laboratory animal core facilities are gratefully acknowledged for their excellent support.

This work was supported by grants from the Deutsche Forschungsgemeinschaft (DFG; project no. 248813719 to M. Felcht; DFG-funded Research Training Group 2099 "Hallmarks of Skin Cancer" [project number 259332240 to H.G. Augustin, M. Felcht, J.S. Utikal, and S. Goerdt]; the DFG-funded Collaborative Research Center CRC1366 "Vascular Control of Organ Function" [project number 39404578 to S. Goerdt and H.G. Augustin]), the European Research Council Advanced Grant "AngioMature" (project 787181 to H.G. Augustin), and the Deutsche Krebshilfe Excellence Program for Established Scientists (project 70114532 to H.G. Augustin).

Author contribution: C. Hübers, A.A. Abdul Pari, D. Grieshober, H.G. Augustin, and M. Felcht conceived and designed the study. C. Hübers, A.A. Abdul Pari, and D. Grieshober performed the majority of the experiments. Further experiments were done by M. Petkov, A. Schmidt, T. Messmer, C.M. Heyer, S. Schölch, S.S. Kapel, B. Schieb, C. Fricke, N. Gengenbacher, M. Singhal, and M. Felcht. R. Will, K. Remans, J.S. Utikal, C. Reissfelder, M. Schlesner, K.M. Hodivala-Dilke, S. Kersten, and S. Goerdt provided data and reagents. C. Hübers, A.A. Abdul Pari, D. Grieshober, H.G. Augustin, and M. Felcht analyzed and interpreted data. C. Hübers, H.G. Augustin, and M. Felcht supervised the project. C. Hübers, A.A. Abdul Pari, D. Grieshober, H.G. Augustin, and M. Felcht prepared the figures and wrote the manuscript. All authors discussed the results and commented on the manuscript.

Disclosures: C. Hübers reported a patent to European Patent Agency no. 19 190 563.7 pending and a patent to European Patent Agency no. 21 156 649.2 pending. A.A. Abdul Pari reported a patent to EP 19 190 563.7 pending and a patent to EP 21 156 649.2 pending. D. Grieshober reported a patent to EP 21 156 649.2 pending. J.S. Utikal is on the advisory board or has received honoraria and travel support from Amgen, Bristol Myers Squibb, GSK, Immunocore, LeoPharma, Merck Sharp and Dohme, Novartis, Pierre Fabre, Roche, and Sanofi outside the submitted work. K.M. Hodivala-Dilke reported personal fees from Ellipses and non-financial support from Vasodynamics outside the submitted work. H.G. Augustin reported a patent to inhibition of metastasis development by nANGPTL-4 pending and a patent to nANGPTL4 as marker for disease progression pending. M. Felcht reported a patent to DKFZ/UHEI patent application "inhibition of metastasis development by nANGPLT4" pending and a patent to DKFZ/UHEI patent application "nANGPLT4 as marker for disease progression" pending. No other disclosures were reported.

Submitted: 4 December 2020
Revised: 7 August 2022
Accepted: 15 September 2022

References

Alieva, M., J. van Rheenen, and M.L.D. Broekman. 2018. Potential impact of invasive surgical procedures on primary tumor growth and metastasis. *Clin. Exp. Metastasis.* 35:319–331. https://doi.org/10.1007/s10585-018-9896-8

Baba, K., Y. Kitajima, S. Miyake, J. Nakamura, K. Wakiyama, H. Sato, K. Okuyama, H. Kitagawa, T. Tanaka, M. Hiraki, et al. 2017. Hypoxia-induced ANGPTL4 sustains tumour growth and anoikis resistance through different mechanisms in scirrhous gastric cancer cell lines. *Sci. Rep.* 7:11127. https://doi.org/10.1038/s41598-017-11769-x

Baker, M., S.D. Robinson, T. Lechertier, P.R. Barber, B. Tavora, G. D'Amico, D.T. Jones, B. Vojnovic, and K. Hodivala-Dilke. 2011. Use of the mouse aortic ring assay to study angiogenesis. *Nat. Protoc.* 7:89–104. https://doi.org/10.1038/nprot.2011.435

Cazes, A., A. Galaup, C. Chomel, M. Bignon, N. Brechot, S. Le Jan, H. Weber, P. Corvol, L. Muller, S. Germain, and C. Monnot. 2006. Extracellular matrix-bound angiopoietin-like 4 inhibits endothelial cell adhesion, migration, and sprouting and alters actin cytoskeleton. *Circ. Res.* 99:1207–1215. https://doi.org/10.1161/01.RES.0000250758.63358.91

Chen, J.W., Y.J. Luo, Z.F. Yang, L.Q. Wen, and L. Huang. 2018. Knockdown of angiopoietin-like 4 inhibits the development of human gastric cancer. *Oncol. Rep.* 39:1739–1746. https://doi.org/10.3892/or.2018.6253

Chiang, A.C., and J. Massagué. 2008. Molecular basis of metastasis. *N. Engl. J. Med.* 359:2814–2823. https://doi.org/10.1056/NEJMra0805239

Chiarella, P., J. Bruzzo, R.P. Meiss, and R.A. Ruggiero. 2012. Concomitant tumor resistance. *Cancer Lett.* 324:133–141. https://doi.org/10.1016/j.canlet.2012.05.021

Costa, R.A., J.C. Cardoso, and D.M. Power. 2017. Evolution of the angiopoietin-like gene family in teleosts and their role in skin regeneration. *BMC Evol. Biol.* 17:14. https://doi.org/10.1186/s12862-016-0859-x

Dagenais, G.R., D.P. Leong, S. Rangarajan, F. Lanas, P. Lopez-Jaramillo, R. Gupta, R. Diaz, A. Avezum, G.B.F. Oliveira, A. Wielgosz, et al. 2020. Variations in common diseases, hospital admissions, and deaths in middle-aged adults in 21 countries from five continents (PURE): A prospective cohort study. *Lancet.* 395:785–794. https://doi.org/10.1016/S0140-6736(19)32007-0

De Rossi, G., M. Vähätupa, E. Cristante, S.E. Liyanage, U. May, L. Pellinen, S. Aittomäki, Z.M. Cordova, M. Pesu, H. Uusitalo-Järvinen, et al. 2019. Syndecan-4 is required for VE-Cadherin trafficking during pathological angiogenesis. *bioRxiv*. (Posted August 19, 2019). https://doi.org/10.1101/736553

Dewey, F.E., V. Gusarova, C. O'Dushlaine, O. Gottesman, J. Trejos, C. Hunt, C.V. Van Hout, L. Habegger, D. Buckler, K.M. Lai, et al. 2016. Inactivating variants in ANGPTL4 and risk of coronary artery disease. *N. Engl. J. Med.* 374:1123–1133. https://doi.org/10.1056/NEJMoa1510926

Dijk, W., and S. Kersten. 2014. Regulation of lipoprotein lipase by Angptl4. *Trends Endocrinol. Metabol.* 25:146–155. https://doi.org/10.1016/j.tem.2013.12.005

Dillekas, H., M.S. Rogers, and O. Straume. 2019. Are 90% of deaths from cancer caused by metastases? *Cancer Med.* 8:5574–5576. https://doi.org/10.1002/cam4.2474

Elfenbein, A., and M. Simons. 2013. Syndecan-4 signaling at a glance. *J. Cell Sci.* 126:3799–3804. https://doi.org/10.1242/jcs.124636

Folkman, J. 2006. Angiogenesis. *Annu. Rev. Med.* 57:1–18. https://doi.org/10.1146/annurev.med.57.121304.131306

Franco, C.A., S. Liebner, and H. Gerhardt. 2009. Vascular morphogenesis: A wnt for every vessel? *Curr. Opin. Genet. Dev.* 19:476–483. https://doi.org/10.1016/j.gde.2009.09.004

Galaup, A., A. Cazes, S. Le Jan, J. Philippe, E. Connault, E. Le Coz, H. Mekid, L.M. Mir, P. Opolon, P. Corvol, et al. 2006. Angiopoietin-like 4 prevents metastasis through inhibition of vascular permeability and tumor cell motility and invasiveness. *Proc. Natl. Acad. Sci. USA*. 103:18721–18726. https://doi.org/10.1073/pnas.0609025103

Galaup, A., E. Gomez, R. Souktani, M. Durand, A. Cazes, C. Monnot, J. Teillon, S. Le Jan, C. Bouleti, G. Briois, et al. 2012. Protection against myocardial infarction and no-reflow through preservation of vascular integrity by angiopoietin-like 4. *Circulation*. 125:140–149. https://doi.org/10.1161/CIRCULATIONAHA.111.049072

Ge, H., G. Yang, L. Huang, D.L. Motola, T. Pourbahrami, and C. Li. 2004. Oligomerization and regulated proteolytic processing of angiopoietin-like protein 4. *J. Biol. Chem.* 279:2038–2045. https://doi.org/10.1074/jbc.M307583200

Goh, Y.Y., M. Pal, H.C. Chong, P. Zhu, M.J. Tan, L. Punugu, C.R.I. Lam, Y.H. Yau, C.K. Tan, R.-L. Huang, et al. 2010. Angiopoietin-like 4 interacts with integrins beta1 and beta5 to modulate keratinocyte migration. *Am. J. Pathol.* 177:2791–2803. https://doi.org/10.2353/ajpath.2010.100129

Gomez Perdiguero, E., A. Liabotis-Fontugne, M. Durand, C. Faye, S. Ricard-Blum, M. Simonutti, S. Augustin, B.M. Robb, M. Paques, D.M. Valenzuela, et al. 2016. ANGPTL4–αvβ3 interaction counteracts hypoxia-induced vascular permeability by modulating Src signalling downstream of vascular endothelial growth factor receptor 2. *J. Pathol.* 240:461–471. https://doi.org/10.1002/path.4805

Hanahan, D., and J. Folkman. 1996. Patterns and emerging mechanisms of the angiogenic switch during tumorigenesis. *Cell*. 86:353–364. https://doi.org/10.1016/s0092-8674(00)80108-7

Hu, K., S. Babapoor-Farrokhran, M. Rodrigues, M. Deshpande, B. Puchner, F. Kashiwabuchi, S.J. Hassan, L. Asnaghi, J.T. Handa, S. Merbs, et al. 2016. Hypoxia-inducible factor 1 upregulation of both VEGF and ANGPTL4 is required to promote the angiogenic phenotype in uveal melanoma. *Oncotarget*. 7:7816–7828. https://doi.org/10.18632/oncotarget.6868

Huang, R.L., Z. Teo, H.C. Chong, P. Zhu, M.J. Tan, C.K. Tan, C.R. Lam, M.K. Sng, D.T. Leong, S.M. Tan, et al. 2011. ANGPTL4 modulates vascular junction integrity by integrin signaling and disruption of intercellular VE-cadherin and claudin-5 clusters. *Blood*. 118:3990–4002. https://doi.org/10.1182/blood-2011-01-328716

Ito, Y., Y. Oike, K. Yasunaga, K. Hamada, K. Miyata, S. Matsumoto, S. Sugano, H. Tanihara, Y. Masuho, and T. Suda. 2003. Inhibition of angiogenesis and vascular leakiness by angiopoietin-related protein 4. *Cancer Res.* 63:6651–6657

Izraely, S., S. Ben-Menachem, O. Sagi-Assif, T. Meshel, D.M. Marzese, S. Ohe, I. Zubrilov, M. Pasmanik-Chor, D.S.B. Hoon, and I.P. Witz. 2017. ANGPTL4 promotes the progression of cutaneous melanoma to brain metastasis. *Oncotarget*. 8:75778–75796. https://doi.org/10.18632/oncotarget.19018

Kirsch, N., L.S. Chang, S. Koch, A. Glinka, C. Dolde, G. Colozza, M.D.J. Benitez, E.M. De Robertis, and C. Niehrs. 2017. Angiopoietin-like 4 Is a Wnt signaling antagonist that promotes LRP6 turnover. *Dev. Cell*. 43:71–82.e6. https://doi.org/10.1016/j.devcel.2017.09.011

Kolb, R., P. Kluz, Z.W. Tan, N. Borcherding, N. Bormann, A. Vishwakarma, L. Balcziak, P. Zhu, B.S. Davies, F. Gourronc, et al. 2019. Obesity-associated inflammation promotes angiogenesis and breast cancer via angiopoietin-like 4. *Oncogene*. 38:2351–2363. https://doi.org/10.1038/s41388-018-0592-6

Korn, C., B. Scholz, J. Hu, K. Srivastava, J. Wojtarowicz, T. Arnsperger, R.H. Adams, M. Boutros, H.G. Augustin, and I. Augustin. 2014. Endothelial cell-derived non-canonical Wnt ligands control vascular pruning in angiogenesis. *Development*. 141:1757–1766. https://doi.org/10.1242/dev.104422

Krall, J.A., F. Reinhardt, O.A. Mercury, D.R. Pattabiraman, M.W. Brooks, M. Dougan, A.W. Lambert, B. Bierie, H.L. Ploegh, S.K. Dougan, and R.A. Weinberg. 2018. The systemic response to surgery triggers the outgrowth of distant immune-controlled tumors in mouse models of dormancy. *Sci. Transl. Med.* 10:eaan3464. https://doi.org/10.1126/scitranslmed.aan3464

Kubo, H., S. Mensurado, N. Goncalves-Sousa, K. Serre, and B. Silva-Santos. 2017. Primary tumors limit metastasis formation through induction of IL15-mediated cross-talk between patrolling monocytes and NK cells. *Cancer Immunol. Res.* 5:812–820. https://doi.org/10.1158/2326-6066.CIR-17-0082

La Paglia, L., A. Listi, S. Caruso, V. Amodeo, F. Passiglia, V. Bazan, and D. Fanale. 2017. Potential role of ANGPTL4 in the cross talk between metabolism and cancer through PPAR signaling pathway. *PPAR Res.* 2017:8187235. https://doi.org/10.1155/2017/8187235

Le Jan, S., C. Amy, A. Cazes, C. Monnot, N. Lamandé, J. Favier, J. Philippe, M. Sibony, J.M. Gasc, P. Corvol, and S. Germain. 2003. Angiopoietin-like 4 is a proangiogenic factor produced during ischemia and in conventional renal cell carcinoma. *Am. J. Pathol.* 162:1521–1528. https://doi.org/10.1016/S0002-9440(10)64285-X

Lei, X., F. Shi, D. Basu, A. Huq, S. Routhier, R. Day, and W. Jin. 2011. Proteolytic processing of angiopoietin-like protein 4 by proprotein convertases modulates its inhibitory effects on lipoprotein lipase activity. *J. Biol. Chem.* 286:15747–15756. https://doi.org/10.1074/jbc.M110.217638

Li, H., C. Ge, F. Zhao, M. Yan, C. Hu, D. Jia, H. Tian, M. Zhu, T. Chen, G. Jiang, et al. 2011. Hypoxia-inducible factor 1 alpha-activated angiopoietin-like protein 4 contributes to tumor metastasis via vascular cell adhesion molecule-1/integrin β1 signaling in human hepatocellular carcinoma. *Hepatology*. 54:910–919. https://doi.org/10.1002/hep.24479

Li, L., H.C. Chong, S.Y. Ng, K.W. Kwok, Z. Teo, E.H.P. Tan, C.C. Choo, J.E. Seet, H.W. Choi, M.L. Buist, et al. 2015. Angiopoietin-like 4 increases pulmonary tissue leakiness and damage during influenza pneumonia. *Cell Rep.* 10:654–663. https://doi.org/10.1016/j.celrep.2015.01.011

Liao, Y.H., K.H. Chiang, J.M. Shieh, C.R. Huang, C.J. Shen, W.C. Huang, and B.K. Chen. 2017. Epidermal growth factor-induced ANGPTL4 enhances anoikis resistance and tumour metastasis in head and neck squamous cell carcinoma. *Oncogene*. 36:2228–2242. https://doi.org/10.1038/onc.2016.371

Love, M.I., W. Huber, and S. Anders. 2014. Moderated estimation of fold change and dispersion for RNA-seq data with DESeq2. *Genome Biol.* 15:550. https://doi.org/10.1186/s13059-014-0550-8

Ma, T., B.C. Jham, J. Hu, E.R. Friedman, J.R. Basile, A. Molinolo, A. Sodhi, and S. Montaner. 2010. Viral G protein-coupled receptor up-regulates Angiopoietin-like 4 promoting angiogenesis and vascular permeability in Kaposi's sarcoma. *Proc. Natl. Acad. Sci. USA*. 107:14363–14368. https://doi.org/10.1073/pnas.1001065107

Mandard, S., F. Zandbergen, N.S. Tan, P. Escher, D. Patsouris, W. Koenig, R. Kleemann, A. Bakker, F. Veenman, W. Wahli, et al. 2004. The direct peroxisome proliferator-activated receptor target fasting-induced adipose factor (FIAF/PGAR/ANGPTL4) is present in blood plasma as a truncated protein that is increased by fenofibrate treatment. *J. Biol. Chem.* 279:34411–34420. https://doi.org/10.1074/jbc.M403058200

Meier, F., S. Will, U. Ellwanger, B. Schlagenhauff, B. Schittek, G. Rassner, and C. Garbe. 2002. Metastatic pathways and time courses in the orderly progression of cutaneous melanoma. *Br. J. Dermatol.* 147:62–70. https://doi.org/10.1046/j.1365-2133.2002.04867.x

Nakayama, T., H. Hirakawa, K. Shibata, K. Abe, T. Nagayasu, and T. Taguchi. 2010. Expression of angiopoietin-like 4 in human gastric cancer: ANGPTL4 promotes venous invasion. *Oncol. Rep.* 24:599–606. https://doi.org/10.3892/or_00000897

Nakayama, T., H. Hirakawa, K. Shibata, A. Nazneen, K. Abe, T. Nagayasu, and T. Taguchi. 2011. Expression of angiopoietin-like 4 (ANGPTL4) in human colorectal cancer: ANGPTL4 promotes venous invasion and distant metastasis. *Oncol. Rep.* 25:929–935. https://doi.org/10.3892/or.2011.1176

Ng, K.T.-P., A. Xu, Q. Cheng, D.Y. Guo, Z.X.-H. Lim, C.K.-W. Sun, J.H.-S. Fung, R.T.-P. Poon, S.T. Fan, C.M. Lo, and K. Man. 2014. Clinical relevance and therapeutic potential of angiopoietin-like protein 4 in hepatocellular carcinoma. *Mol. Cancer*. 13:196. https://doi.org/10.1186/1476-4598-13-196

O'Reilly, M.S., T. Boehm, Y. Shing, N. Fukai, G. Vasios, W.S. Lane, E. Flynn, J.R. Birkhead, B.R. Olsen, and J. Folkman. 1997. Endostatin: An endogenous inhibitor of angiogenesis and tumor growth. *Cell*. 88:277–285. https://doi.org/10.1016/s0092-8674(00)81848-6

O'Reilly, M.S., L. Holmgren, Y. Shing, C. Chen, R.A. Rosenthal, M. Moses, W.S. Lane, Y. Cao, E.H. Sage, and J. Folkman. 1994. Angiostatin: A novel angiogenesis inhibitor that mediates the suppression of metastases by a Lewis lung carcinoma. *Cell*. 79:315–328. https://doi.org/10.1016/0092-8674(94)90200-3

Okochi-Takada, E., N. Hattori, T. Tsukamoto, K. Miyamoto, T. Ando, S. Ito, Y. Yamamura, M. Wakabayashi, Y. Nobeyama, and T. Ushijima. 2014. ANGPTL4 is a secreted tumor suppressor that inhibits angiogenesis. *Oncogene*. 33:2273–2278. https://doi.org/10.1038/onc.2013.174

Padua, D., X.H. Zhang, Q. Wang, C. Nadal, W.L. Gerald, R.R. Gomis, and J. Massague. 2008. TGFbeta primes breast tumors for lung metastasis seeding through angiopoietin-like 4. *Cell*. 133:66–77. https://doi.org/10.1016/j.cell.2008.01.046

Piranlioglu, R., E. Lee, M. Ouzounova, R.J. Bollag, A.H. Vinyard, A.S. Arbab, D. Marasco, M. Guzel, J.K. Cowell, M. Thangaraju, et al. 2019. Primary tumor-induced immunity eradicates disseminated tumor cells in syngeneic mouse model. *Nat. Commun.* 10:1430. https://doi.org/10.1038/s41467-019-09015-1

Qin, Y., A. Dinabandhu, X. Cao, J.C. Sanchez, K. Jee, M. Rodrigues, C. Guo, J. Zhang, J. Vancel, D. Menon, et al. 2022. ANGPTL4 influences the therapeutic response of patients with neovascular age-related macular degeneration by promoting choroidal neovascularization. *JCI Insight*. 7: 157896. https://doi.org/10.1172/jci.insight.157896

Rao, N., Y.F. Lee, and R. Ge. 2015. Novel endogenous angiogenesis inhibitors and their therapeutic potential. *Acta Pharmacol. Sin.* 36:1177–1190. https://doi.org/10.1038/aps.2015.73

Reisinger, E., L. Genthner, J. Kerssemakers, P. Kensche, S. Borufka, A. Jugold, A. Kling, M. Prinz, I. Scholz, G. Zipprich, et al. 2017. OTP: An automatized system for managing and processing NGS data. *J. Biotechnol.* 261: 53–62. https://doi.org/10.1016/j.jbiotec.2017.08.006

Rong, B., S. Yang, W. Li, W. Zhang, and Z. Ming. 2012. Systematic review and meta-analysis of Endostar (rh-endostatin) combined with chemotherapy versus chemotherapy alone for treating advanced non-small cell lung cancer. *World J. Surg. Oncol.* 10:170. https://doi.org/10.1186/1477-7819-10-170

Shafik, N.M., D.A. Mohamed, A.E. Bedder, and A.M. El-Gendy. 2015. Significance of tissue expression and serum levels of angiopoietin-like protein 4 in breast cancer progression: Link to NF-κB/P65 activity and pro-inflammatory cytokines. *Asian Pac. J. Cancer Prev. APJCP*. 16:8579–8587. https://doi.org/10.7314/apjcp.2015.16.18.8579

Shibata, K., T. Nakayama, H. Hirakawa, S. Hidaka, and T. Nagayasu. 2010. Clinicopathological significance of angiopoietin-like protein 4 expression in oesophageal squamous cell carcinoma. *J. Clin. Pathol.* 63: 1054–1058. https://doi.org/10.1136/jcp.2010.078600

Sodhi, A., T. Ma, D. Menon, M. Deshpande, K. Jee, A. Dinabandhu, J. Vancel, D. Lu, and S. Montaner. 2019. Angiopoietin-like 4 binds neuropilins and cooperates with VEGF to induce diabetic macular edema. *J. Clin. Invest.* 129:4593–4608. https://doi.org/10.1172/JCI120879

Stoletov, K., P.H. Beatty, and J.D. Lewis. 2020. Novel therapeutic targets for cancer metastasis. *Expet Rev. Anticancer Ther.* 20:97–109. https://doi.org/10.1080/14737140.2020.1718496

Sund, M., Y. Hamano, H. Sugimoto, A. Sudhakar, M. Soubasakos, U. Yerramalla, L.E. Benjamin, J. Lawler, M. Kieran, A. Shah, and R. Kalluri. 2005. Function of endogenous inhibitors of angiogenesis as endothelium-specific tumor suppressors. *Proc. Natl. Acad. Sci. USA*. 102:2934–2939. https://doi.org/10.1073/pnas.0500180102

Tan, M.J., Z. Teo, M.K. Sng, P. Zhu, and N.S. Tan. 2012. Emerging roles of angiopoietin-like 4 in human cancer. *Mol. Cancer Res.* 10:677–688. https://doi.org/10.1158/1541-7786.MCR-11-0519

Tang, Z., F. Zhang, Y. Li, P. Arjunan, A. Kumar, C. Lee, and X. Li. 2011. A mouse model of the cornea pocket assay for angiogenesis study. *J. Vis. Exp.* 18:3077. https://doi.org/10.3791/3077

Tian, L., J. Zhou, M.C. Casimiro, B. Liang, J.O. Ojeifo, M. Wang, T. Hyslop, C. Wang, and R.G. Pestell. 2009. Activating peroxisome proliferator-activated receptor gamma mutant promotes tumor growth in vivo by enhancing angiogenesis. *Cancer Res.* 69:9236–9244. https://doi.org/10.1158/0008-5472.CAN-09-2067

Tohme, S., R.L. Simmons, and A. Tsung. 2017. Surgery for cancer: A trigger for metastases. *Cancer Res.* 77:1548–1552. https://doi.org/10.1158/0008-5472.CAN-16-1536

Vlodavsky, I., J. Folkman, R. Sullivan, R. Fridman, R. Ishai-Michaeli, J. Sasse, and M. Klagsbrun. 1987. Endothelial cell-derived basic fibroblast growth factor: Synthesis and deposition into subendothelial extracellular matrix. *Proc. Natl. Acad. Sci. USA*. 84:2292–2296. https://doi.org/10.1073/pnas.84.8.2292

Wang, Z., B. Han, Z. Zhang, J. Pan, and H. Xia. 2010. Expression of angiopoietin-like 4 and tenascin C but not cathepsin C mRNA predicts prognosis of oral tongue squamous cell carcinoma. *Biomarkers*. 15:39–49. https://doi.org/10.3109/13547500903261362

Welch, D.R., and D.R. Hurst. 2019. Defining the hallmarks of metastasis. *Cancer Res.* 79:3011–3027. https://doi.org/10.1158/0008-5472.CAN-19-0458

Westphal, J.R. 2004. Technology evaluation: ABT-510, abbott. *Curr. Opin. Mol. Ther.* 6:451–457

Wu, T., E. Hu, S. Xu, M. Chen, P. Guo, Z. Dai, T. Feng, L. Zhou, W. Tang, L. Zhan, et al. 2021. clusterProfiler 4.0: A universal enrichment tool for interpreting omics data. *Innovation*. 2:100141. https://doi.org/10.1016/j.xinn.2021.100141

Yang, X., Y. Cheng, and G. Su. 2018. A review of the multifunctionality of angiopoietin-like 4 in eye disease. *Biosci. Rep.* 38:BSR20180557. https://doi.org/10.1042/BSR20180557

Zhang, T., A. Kastrenopoulou, Q. Larrouture, N.A. Athanasou, and H.J. Knowles. 2018. Angiopoietin-like 4 promotes osteosarcoma cell proliferation and migration and stimulates osteoclastogenesis. *BMC Cancer*. 18:536. https://doi.org/10.1186/s12885-018-4468-5

Zhu, P., M.J. Tan, R.-L. Huang, C.K. Tan, H.C. Chong, M. Pal, C.R.I. Lam, P. Boukamp, J.Y. Pan, S.H. Tan, et al. 2011. Angiopoietin-like 4 protein elevates the prosurvival intracellular O_2^-: H_2O_2 ratio and confers anoikis resistance to tumors. *Cancer Cell*. 19:401–415. https://doi.org/10.1016/j.ccr.2011.01.018

JEM

Supplemental material

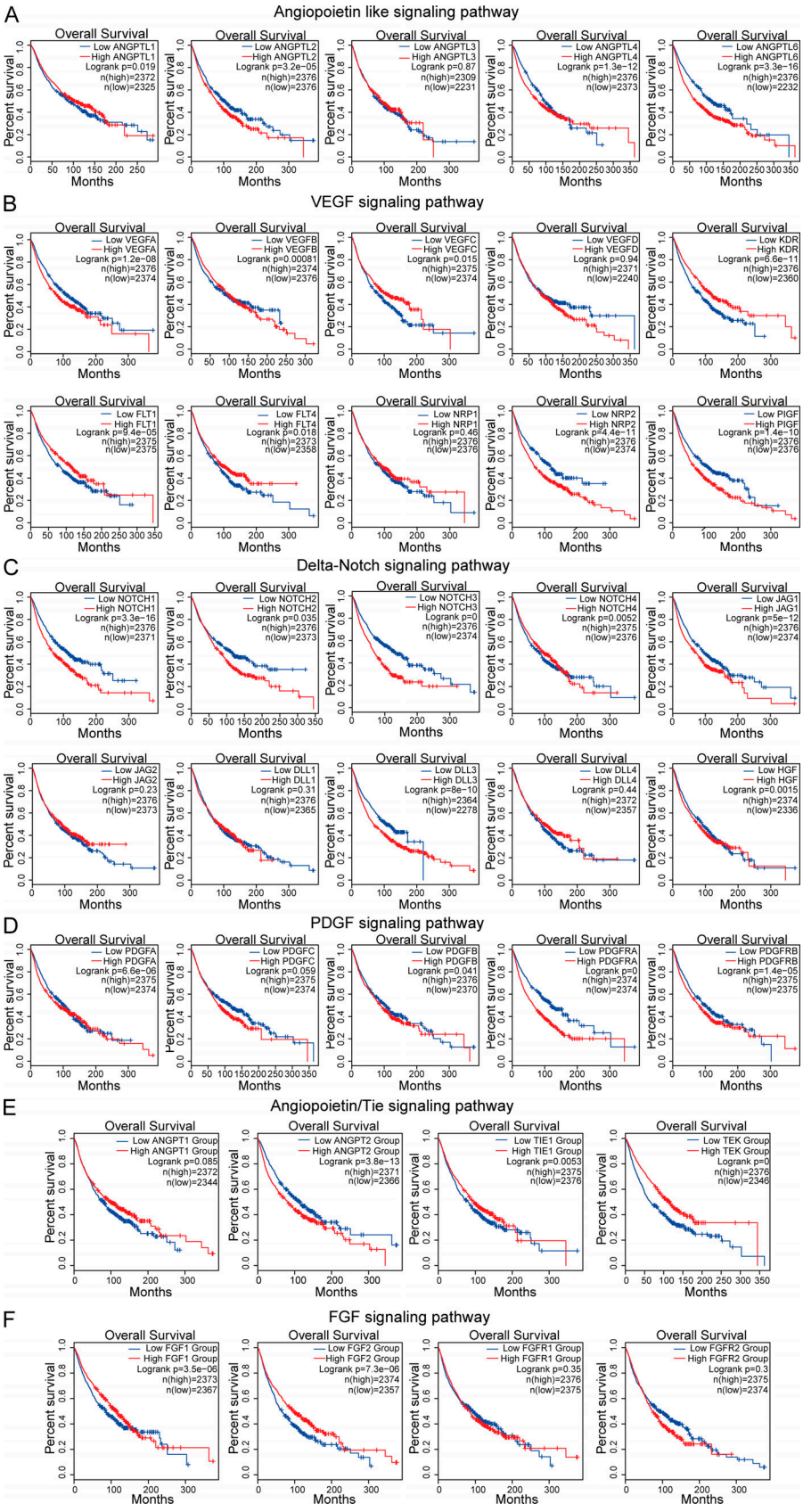

Figure S1. **Overall survival analysis of key angiogenic molecules in 32 tumor entities. (A–F)** Kaplan–Meier plots depicting the overall survival of molecules belonging to (A) angiopoetin-like signaling pathway, (B) VEGF-A signaling pathway, (C) Delta-Notch signaling pathway, (D) PDGF signaling pathway, (E) angiopoetin/Tie signaling pathway, and (F) FGF signaling pathway.

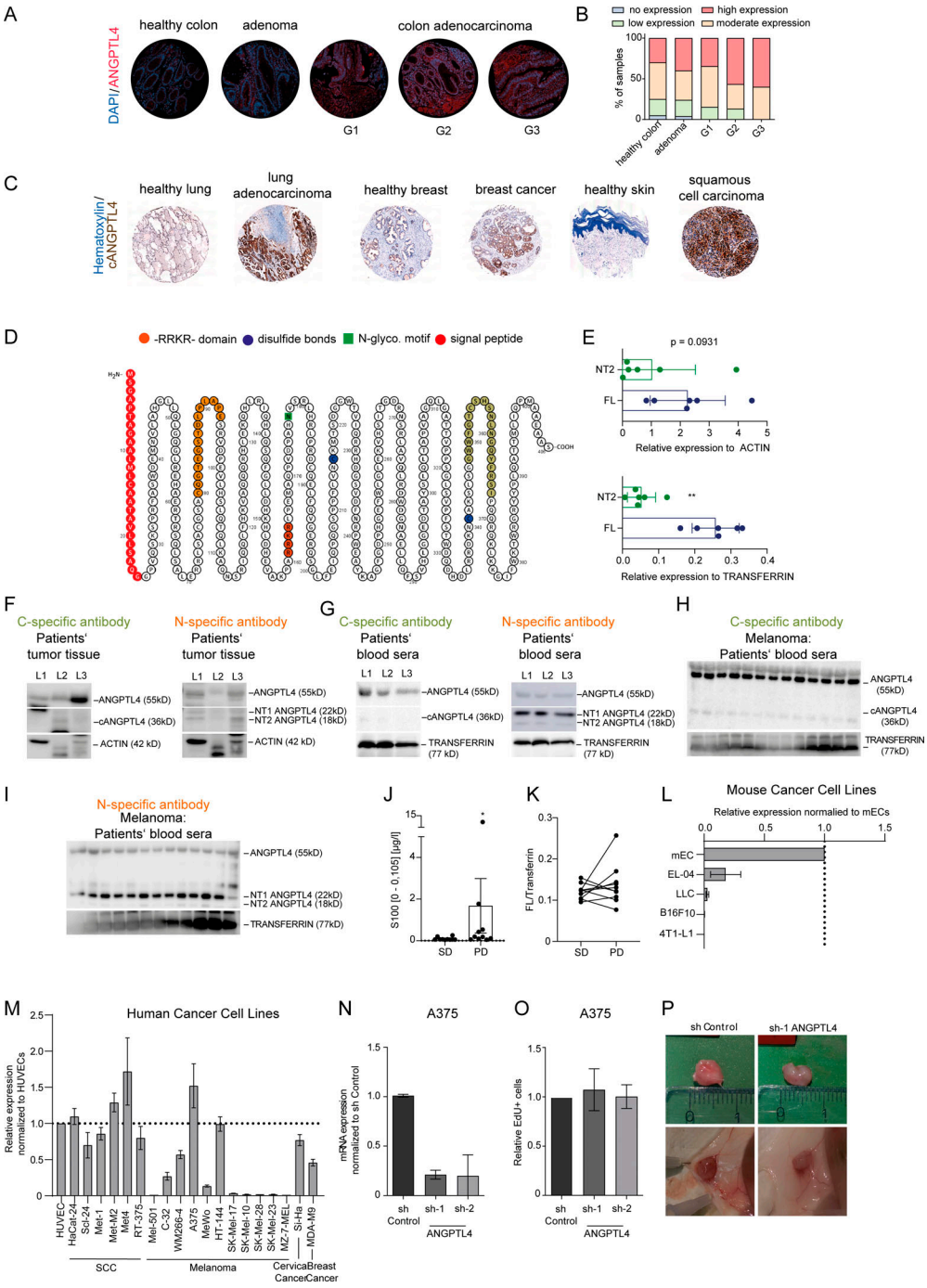

Figure S2. **Tracing and characterizing the functional role of ANGPTL4 in clinical and preclinical settings. (A)** Representative IF images of healthy colon, adenoma, and different grades of colon adenocarcinoma tissue sections (G1, G2, and G3) stained with ANGPTL4 antibody. **(B)** Quantification of no, low, moderate, and high ANGPTL4 protein expression in healthy colon (n = 20), adenoma (n = 25), and different grades of colon carcinoma (n = 69) tissue sections. **(C)** Representative stitched tile scanned IHC images of lung adenocarcinoma, breast cancer, cSCC, and corresponding healthy tissue sections stained with ANGPTL4 antibody. **(D)** Schematic illustration of the amino acid sequence of ANGPTL4. The protein sequence was visualized with the Protter software. **(E)** Graphs showing the densitometry quantitation of the Western blots from Fig. 1, E and G. Protein levels were normalized to actin in melanoma tumors and to transferrin in patients' sera (n = 6; mean ± SD). **, P < 0.01, Mann–Whitney U test. **(F and G)** Western blotting with a cANGPTL4-specific antibody and an nANGPTL4-specific antibody in indexed lung cancer tumors and serum samples (n = 3). **(H and I)** Western blotting of melanoma patients' sera with a C-specific antibody (I) and an N-specific antibody (n = 13). **(J)** Quantitation of S100 levels in melanoma patients' sera with either stable disease (SD) or progressive disease (PD) diagnosis (n = 10; mean ± SD). *, P < 0.05, Mann–Whitney U test. **(K)** Densitometric quantitation of protein levels of Western blots (Fig. 2 C) was performed with Fiji. The graph shows the NT2/ANGPTL4 ratio normalized to transferrin in patients' sera with either stable disease (SD) or progressive disease (PD) diagnosis (n = 10). **(L and M)** A systematic screen of the endogenous ANGPLT4 levels in different murine (L) and human (M) tumor cell lines analyzed by RT-qPCR (n = 3; mean ± SD). **(N)** *ANGPTL4* expression in control and *ANGPTL4* knockdown A375 tumor cell line quantified by RT-qPCR (n = 2; mean ± SD). **(O)** Quantitation of cellular proliferation of A375 sh Control and sh*ANGPTL4* analyzed by EdU flow cytometry assay (n = 4; mean ± SD). **(P)** Representative images of size-matched A375 sh Control and sh*ANGPTL4* tumors at the time of excision. Source data are available for this figure: SourceData FS2.

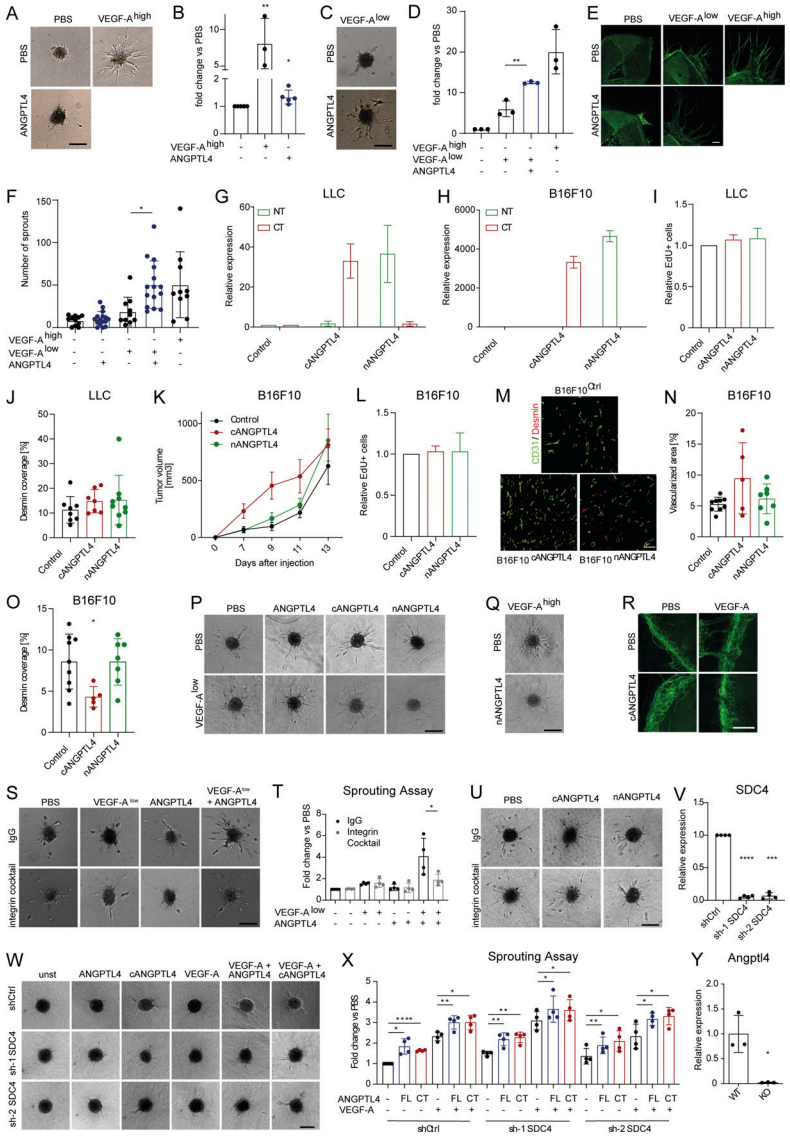

Figure S3. **Differential functions of ANGPTL4 and its cleavage fragments. (A)** Representative images of the spheroid sprouting assay with either VEGF-A or ANGPTL4 mono-stimulation. Scale bar: 200 µm. **(B)** Quantitation of the cumulative sprout length (n = 3–5; mean ± SD). *, P < 0.05; **, P < 0.01, two-tailed paired Student's t test. **(C)** Representative pictures of the spheroid sprouting assay with 400 ng/ml ANGPTL4 in combination with a subcritical dose of VEGF-A. Scale bar: 200 µm. **(D)** The graph shows the quantitation of the cumulative sprout length (n = 3; mean ± SD). **, P < 0.01, two-tailed paired Student's t test. **(E)** Representative IF images of the aortic ring assay stained with FITC-lectin. Scale bar: 100 µm. **(F)** The graph depicts the quantitation of the number of sprouts per aortic ring (n = 11–17; mean ± SD). *, P < 0.05, two-tailed unpaired Student's t test. **(G)** *Angptl4* expression in control, nANGPTL4-, and cANGPTL4-overexpressing LLC tumor cells quantified by RT-qPCR (n = 3; mean ± SEM). **(H)** *Angptl4* expression in control, nANGPTL4-, and cANGPTL4-overexpressing B16F10 tumor cells quantified by RT-qPCR (n = 2; mean ± SEM). **(I)** Quantitation of cellular proliferation of control, nANGPTL4-, and cANGPTL4-overexpressing LLC tumor cells analyzed by EdU flow cytometry assay (n = 4; mean ± SD). **(J)** Quantitation of Desmin coverage in control, nANGPTL4-, and cANGPTL4-overexpressing LLC primary tumors (n = 7–9; mean ± SD). **(K)** Growth kinetics of control, nANGPTL4-, or cANGPTL4-overexpressing B16F10 primary tumors (n = 6–10; mean ± SEM). **(L)** Quantitation of cellular proliferation of control, nANGPTL4-, and cANGPTL4-overexpressing B16F10 tumor cells analyzed by EdU flow cytometry assay (n = 4; mean ± SD). **(M)** Representative IF images of B16F10 tumor sections co-stained with CD31 (in green) and Desmin (in red). Scale bar: 100 µm. **(N and O)** Quantitation of vascularized area (N) and Desmin coverage (O) in control, nANGPTL4-, and cANGPTL4-overexpressing B16F10 primary tumors (n = 5–9; mean ± SD). *, P < 0.05, unpaired Student's t test. **(P and Q)** Representative images of EC spheroids (Fig. 4 A) stimulated with the mentioned cytokines. Scale bar: 200 µm. **(R)** Representative stitched tile scanned IF images of the corneas isolated from C57BL/6J mice stimulated with the indicated cytokines. Corneas were stained for the EC marker CD31 (green). Scale bar: 500 µm. **(S)** Representative images of IgG or integrin-blocking antibody treated EC spheroids stimulated with ANGPTL4, VEGF-A, or a combination thereof. Scale bar: 200 µm. **(T)** Quantitation of the cumulative sprout length of IgG or integrin-blocking antibody-treated EC spheroids stimulated with ANGPTL4, VEGF-A, or a combination thereof (n = 4; mean ± SD). *, P < 0.05, paired Student's t test. **(U)** Representative images of IgG or integrin-blocking antibody treated EC spheroids stimulated with the indicated cytokines. Scale bar: 200 µm. **(V)** *SDC4* expression in control and *SDC4* knockdown HUVECs quantified by RT-qPCR (n = 4; mean ± SD). ***, P < 0.001; ****, P < 0.0001, two-tailed paired Student's t test. **(W)** Representative images of EC spheroids stimulated with the mentioned cytokines. Scale bar: 200 µm. **(X)** Quantitation of the cumulative sprout length of EC spheroids of sh control (non-targeting) and SDC4-silenced EC spheroids stimulated with the indicated cytokines (n = 5; mean ± SD). *, P < 0.05; **, P < 0.01; ****, P < 0.0001, two-tailed paired Student's t test. **(Y)** Quantitation of *Angptl4* expression in whole liver lysates of WT and *Angptl4*-deficient (KO) mice (n = 3; mean ± SD). *, P < 0.05, unpaired Student's t test.

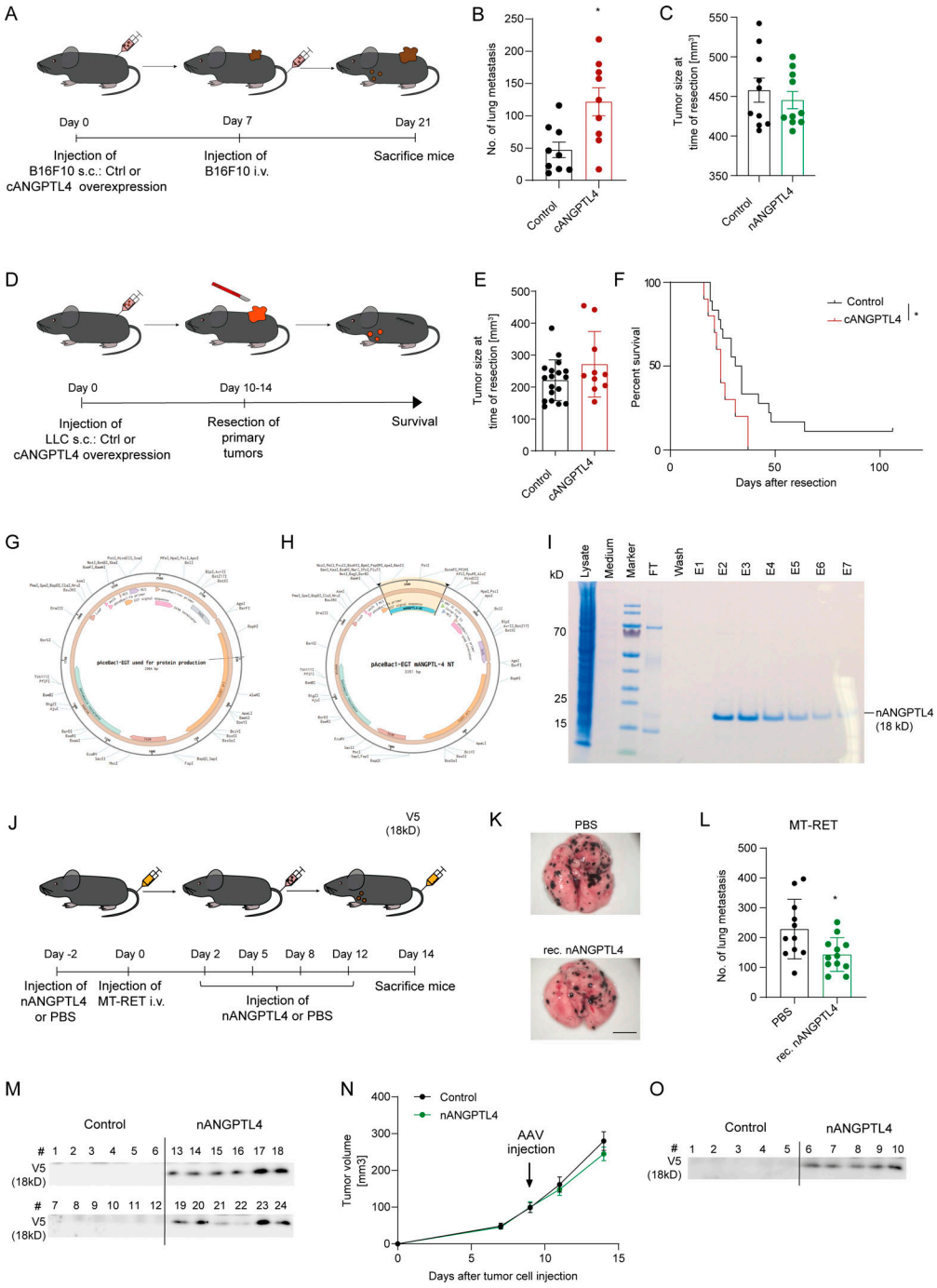

Figure S4. **Proteolytically cleaved fragments of ANGPTL4 differentially regulate metastasis. (A)** Schematic representation of experimental design to study the effect of systemic cANGPTL4 on lung metastasis. **(B)** The graph represents the quantitation of metastatic lung foci (n = 9; mean ± SEM). *, P < 0.05, Mann–Whitney U test. **(C)** Tumor volume at the time of tumor resection of control and nANGPTL4-overexpressing LLC primary tumors (n = 10; mean ± SEM). **(D)** Schematic representation of the LLC postsurgical metastasis model. **(E)** Tumor volume at the time of tumor resection of control and cANGPTL4-overexpressing LLC primary tumors (n = 10–18; mean ± SD). **(F)** Kaplan–Meier plot showing percent survival of mice implanted with either control or cANGPTL4-overexpressing LLC tumor cells after primary tumor resection (n = 10–18). *, P < 0.05, log-rank (Mantel–Cox) test. **(G and H)** Vector map of empty backbone plasmid (pAceBac-EGT; G) and (H) plasmid construct used for generating recombinant mouse nANGPTL4. **(I)** SDS-PAGE analysis of nANGPTL4-expressing insect cells lysate, cell culture medium, flow through (FT) from StrepTactinXT column, wash solution used in StrepTactinXT column and successive eluates (E1-E7) from StrepTactinXT column. Probes were resolved on a gradient gel (4–12%) and stained with Coomassie blue. **(J)** Schematic representation of the MT-RET experimental metastasis model to evaluate the therapeutic efficacy of recombinant nANGPTL4. Mice were injected with recombinant nANGPTL4 (7 µg/shot) or PBS as depicted in the scheme. **(K)** Representative images of metastatic lung foci from mice treated with PBS or nANGPTL4. Scale bar: 2 mm. **(L)** Graph representing the quantitation of metastatic foci (n = 11; mean ± SD). *, P ≤ 0.05, Mann–Whitney U test. **(M)** Western blot from mouse sera that were taken at the endpoint of B16F10 experimental metastasis model. V5-tagged nANGPTL4 was detected using the anti-V5 antibody. **(N)** Growth kinetics of LLC tumors in control or nANGPTL4 AAV-injected mice (n = 13; mean ± SEM). **(O)** Western blot of mouse sera that were taken at the endpoint of LLC postsurgical metastasis model. V5-tagged nANGPTL4 was detected using the anti-V5 antibody. Source data are available for this figure: SourceData FS4.

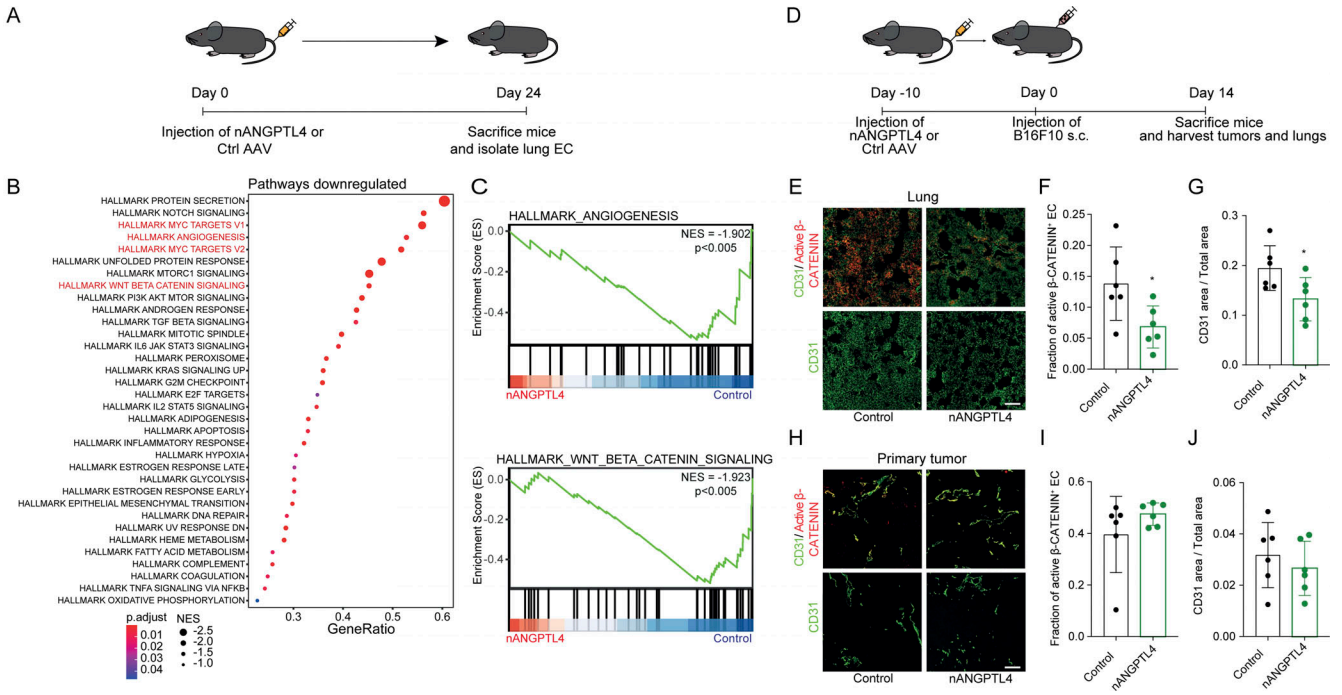

Figure S5. **nANGPTL4 perturbs angiogenesis and WNT signaling at the metastatic site. (A)** Schematic representation of the RNAseq experiment with AAV mediated upregulation of nANGPTL4 or control. **(B)** GSEA of pathways downregulated after nANGPTL4 treatment. NES, normalized enrichment score. **(C)** GSEA plots showing regulated hallmark pathways in nANGPTL4-treated lung EC. **(D)** Schematic representation of the B16F10 primary tumor experiment with AAV mediated upregulation of nANGPTL4 or control. **(E)** Representative images of lung sections co-stained with CD31 (green) and active β-catenin (red). Scale bar: 100 µm. **(F and G)** Quantitation of active β-catenin positive ECs (F) and CD31 (G) in lungs of mice with systemic overexpression of control or nANGPTL4 AAV (n = 6; mean ± SD). *, P < 0.05, Mann–Whitney U test. **(H)** Representative images of B16F10 tumors sections stained co-stained with CD31 (green) and active β-catenin (red). Scale bar: 100 µm. **(I and J)** Immunofluorescence based quantitation of active β-catenin positive ECs and CD31 (J) in primary tumors of mice with systemic overexpression of control or nANGPTL4 AAV (n = 6; mean ± SD).

Table S1 is provided online and illustrates the clinicopathological data of the patients included in this study.